Active-screen plasma surface multi-functionalisation of biopolymers and carbon-based materials – an overview

Dashtbozorg, Behnam; Tao, Xiao; Dong, Hanshan

DOI:
10.1016/j.surfcoat.2022.128188

Surface & Coatings Technology 442 (2022) 128188

Contents lists available at ScienceDirect

Surface & Coatings Technology

journal homepage: www.elsevier.com/locate/surfcoat

Active-screen plasma surface multi-functionalisation of biopolymers and carbon-based materials – An overview

Behnam Dashtbozorg, Xiao Tao *, Hanshan Dong

School of Metallurgy and Materials, University of Birmingham, Birmingham B15 2TT, UK

ARTICLE INFO

Keywords:
Active-screen plasma
Functionalisation
Biopolymers
Graphene oxide
Carbon fibre
Carbon nanofibre

ABSTRACT

Biopolymer and carbon-based materials have found widespread applications, spanning across different industries, including the medical, energy storage, wind energy, and aerospace sectors. The increasing popularity of both types of materials in industry has created a driving force for the enhancement of their properties to meet the current and future requirements. Active-screen plasma (ASP) has attracted much attention as a versatile and powerful surface engineering solution to meet these growing demands, owing to its treatment uniformity, remote plasma nature, capability for treating both electrically conductive and insulating materials, ability to functionalise surfaces, and the unique combined function of surface activation and deposition (CFAD). Through the introduction of moieties, modification of chemical bonding, change of morphology, and improvement in wettability on the treated surfaces, recent studies have demonstrated the ability for ASP treatments to enhance the biocompatibility of biopolymers. Moreover, ASP has also been tested (and 'bespoke' ASP techniques developed) for advanced carbon-based materials for tailored applications with promising property/performance enhancements, including a) enhanced wettability and interfacial shear strength for carbon fibres in polymer matrix composites, b) improved catalyst layer growth on carbon paper, c) improved electrical conductivity and capacitive performance for carbon nanofibers, and d) enhanced electric and electrochemical properties for graphene oxide.

This review evaluates the recent achievements and findings of ASP treatments performed on biopolymers and carbon-based materials from the Surface Engineering group in the University of Birmingham. The current status of ASP surface multi-functionalisation is communicated, along with the future research focus for materials with poor electrical conductivity and/or vulnerability to degradation.

1. Introduction

Plasma, being the fourth state of matter (after solids, liquids and gases), was initially identified by William Crooks in 1879 as "radiant matter" and then named as "plasma" by Irvine Langmuir in 1923 [1]. However, credit for the work leading up to this discovery also go to numerous notable researchers from the 16th and 17th centuries, including William Gilbert, Charles-François de Cisternay du Fay, Ewald Jürgen von Kleist, Andreas Cunaeu, Abbé Nollet, Charles Cavendish, Benjamin Franklin and Joseph Priestley, who all worked on the fundamentals of electricity and the formation of arc discharges, laying the foundations for the later identification, description and exploitation of plasma-based technologies [2–5]. Thermal plasma can be generated by heating substances to several thousand Kelvin (e.g. solar corona, where electrons and gases are at similar temperatures). On the other hand, non-thermal plasma (or non-equilibrium plasma) is where electrons possess high kinetic energy while larger ions or neutrals remain at relatively low temperatures, thus requiring less input energy and generating less total heat, and therefore is often employed in surface engineering technologies, typically for surface modifications [6,7]. In this regard, after (partial) ionisation, plasma can be considered as conductive gas which contains species physico-chemically more 'active', such as ions, radicals and neutrals (as well as electrons, photons, X-rays, etc.), that can be exploited to modify engineering surfaces with limited, or in complete absence of, damage/influence to the underlying substrate material.

Industrial plasma technologies can be broadly divided into atmospheric pressure plasma (APP) and low-pressure plasma (LPP). APP can be generated, in the absence of vacuum conditions, through direct current (DC) glow discharge [8,9], corona discharge [10], and quite popularly, under dielectric barrier discharge [11–14], where the

* Corresponding author.
E-mail address: x.tao@bham.ac.uk (X. Tao).

https://doi.org/10.1016/j.surfcoat.2022.128188

Available online 2 February 2022

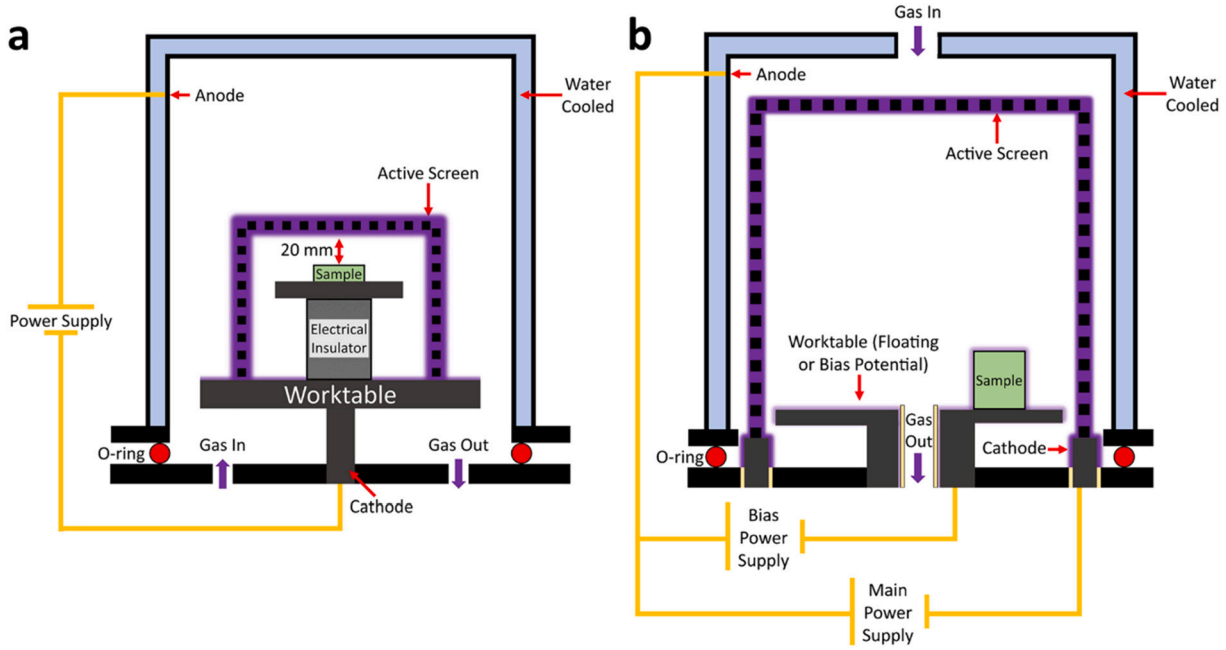

Fig. 1. Schematic illustrations for active-screen plasma configurations, where the sample is held at a) floating potential (in a modified Klöckner DC plasma furnace), and b) floating potential or negatively biased (in an industrial active-screen plasma furnace).

atmospheric pressure working conditions give rise to various benefits (e.g. lower equipment costs, remote operation, and ease of integration into existing 'roll-to-roll' manufacturing lines). A variety of "cold" atmospheric plasma technologies have subsequently emerged, including "diffuse coplanar surface barrier discharge" [15,16], "plasma jet" [17,18] and "micro-plasma" [19–21]), and have attracted extensive attention for surface modification due to their capabilities for retaining gas temperature at near room temperature. Nevertheless, oxidation and surface property degradation can be an issue during APP treatments of some materials. Compared with APP techniques, LPP treatments offer an alternative scalable surface modification approach (i.e. batch production, for simultaneously treating large quantities with varying geometries), with an extra level of process 'cleanliness' and treatment uniformity, while also allowing the use of specific gas atmospheres capable of achieving enhancements necessary for high-end industrial applications.

Conventional LPP can be achieved via applying a DC potential between two conductive plates in an evacuated chamber [1,6,7,22]. However, such conventional low-pressure DC plasma configurations require electrically conductive workpieces, which exhibit strong plasma-surface interactions (such as ionic bombardment) and result in a substantial rise in temperature (e.g. $>$ 200 °C) during treatment. In addition to other limitations, such as arcing, hollow cathode formations and edge effects [6,23,24], these conventional DC plasma treatments are not suitable for materials that are electrically non-conductive and/or vulnerable to low-temperature degradation. LPP treatments of non-conductive materials can be realised via radio frequency and microwave plasma; however, they require more sophisticated processing and significantly higher equipment capital (as reviewed by Corujeira Gallo et al. [25]).

To overcome the problems associated with DC plasma treatment of materials, an alternative approach to plasma treatment was adopted in the early 1990s, labelled as active-screen plasma (ASP) treatments [26]. Under ASP treatment conditions, rather than applying the cathodic potential directly to the workpiece, as is the case under DC plasma treatments, materials to be treated are held at floating potentials or at a small negative bias (as shown in the two configurations demonstrated in Fig. 1). Under ASP conditions, a metal cage consisting of a cylinder screen and lid with perforated holes – collectively known as the active-screen (AS) – enclose the workpiece to be treated, and are subjected to the high cathodic potential during treatment [27,28]. The strong plasma-surface interactions (as during DC plasma) are redirected from the workpiece to the active-screen system during ASP treatments, leading to some profound influences, including [29–37]:

1. Effective reduction or avoidance of surface damage to the workpiece due to the remote plasma nature.
2. Workpieces no longer required to be electrically conductive, such that electrically insulating materials (such as polymers and ceramics) can be treated/functionalised.
3. Effective removal of inhomogeneous plasma heating of workpieces (resulting from hollow cathode formations and/or edge effects).
4. Uniform heating of the workpiece can be achieved through thermal radiation from the active-screen.
5. Deposition of nano/micro particles can be achieved via a "sputtering-deposition" mechanism [28,29,32,38] from the active-screen, which can be integrated with 'sputtering targets'.
6. Introduction of additional treatment variables (e.g. active-screen to workpiece distance, active-screen configuration, and 'sputtering target' materials and configurations).

Adjustment of ASP treatment conditions can enable achievment of bespoke surface modification outcomes, with some controllable or measurable variables being listed in Tables 1 & 2 (namely, temperature, duration, gas pressure, gas mixture and distance between AS and the surface to be treated). The effect of treatment temperature and time are relatively straightforward and more or less equivalent to those described in other metallurgical processes (e.g. heat treatments) [39]. The working gas mixture and pressure also have profound effects on the eventual surface modifications. Gases such as H_2 and Ar contribute to the generation of the plasma and etching/sputtering of material surfaces in situ [24,40,41]. The use of 'reactive' gases such as N_2, O_2 or CH_4, which contain elements such as nitrogen, oxygen or carbon, provide the basis for chemical modifications of surfaces, through either: a) addition of functional groups at low temperatures (e.g. <200 °C) and/or short treatment durations (e.g. <2 h), or b) introduction of 'thick' diffusion-

Table 1
ASP treatments for biopolymer materials.

Ref.	Materials	ASP treatment conditions[a]	Characterisation	
			Physical/chemical	Biological
2010, Kaklamani, et al. [66]	UHMWPE	at 120 °C for 10–60 min, 250 Pa, 75% H_2 + 25% N_2, no distance from top AS lid mentioned	FTIR, XPS, SEM, nanoindentation, laser interferometry	Biocompatibility assessment of 3T3 fibroblasts after 4 days incubation.
2012, Fu, et al. [68]	PCL	at 50 °C for 10 min, 200 Pa, 75% H_2 + 25% N_2, 10 mm distance from top AS lid	FTIR, XPS, wettability	Cell attachment assessment of MC3T3-E1 osteoblast-like after 1 h incubation; self-degradation testing in PBS (phosphate-buffered saline) & lipase from *Pseudomonas cepacian*.
2012, Fu, et al. [69]	Polyurethane	at 80–130 °C for 30 min, 200 Pa, 75% H_2 + 25% N_2, 15 mm distance from top AS lid	SEM, AFM, XPS, FTIR, DSC (differential scanning calorimetry), surface profilometry, wettability	/
2013, Kaklamani, et al. [70]	UHMWPE	at 90 °C for 10–60 min, 250 Pa, 80% N_2 + 20% H_2, 10 mm distance from top AS lid	SEM, XPS, AFM (topographical & adhesive properties), laser interferometry, nanoindentation	(1) Stability assessment in air, PBS or supplemented DMEM (Dulbecco's modified Eagle's medium) for up to 28 days. (2) Biocompatibility assessment of NIH 3T 3 fibroblasts for up to 28 days incubation. (3) MTT metabolic activity assays performed on NIH 3T3 fibroblast incubated surfaces at days 0, 7, 14 and 28.
2013, Kaklamani, et al. [71]	Aluminosilicate glass	at 400 °C for 60 min, 250 Pa, 75% H_2 + 25% N_2, 12 mm distance from top AS lid	SEM, XPS, nanoindentation, laser interferometry,	Biocompatibility assessment of NIH 3T3 fibroblasts after 4 days incubation.
2021, Mehrban, et al. [72]	POSS-PCUU	at <60 °C for 5 min, 75 Pa, 20 mm distance from top AS lid, and gas mixtures of: (1) 100% air, (2) 100% N_2, (3) 100% H_2, (4) 50% H_2 + 50% N_2, (5) 50% H_2 + 50% air	SEM, AFM, XPS, wettability, optical microscopy, optical interferometry	(1) Cell differentiation assessment of human respiratory epithelial cell (HEC) over 28 days (2) Ciliation of HECs after 28 days of culture, and assessment of cilia beat pattern.

[a] Workpieces are under floating potential in all studies.

Table 2
ASP treatments for carbon-based materials.

	Ref.	Materials	ASP treatment conditions[a]	Characterisations
For increased wettability, interfacial bonding and mechanical properties	2017, Corujeira Gallo, et al. [118]	CFs (Torayca® T-700012k-60E) and vitreous C disk (Almath Crucibles, VCR6100)	at <100 °C for 5–40 min, 50 Pa, 75% H_2 + 25% Ar, 15 mm from top AS lid	OES, SEM, AFM, XPS, WCA
	2020, Semitekolos, et al. [119]	CFs (Teijin Tenax HTA-40)	at 17–95 °C for 5 min, 75 Pa, 25% N_2 + 75% H_2 and 5% Ar + 23.75% N_2 + 71.25% H_2, 150 mm to side AS cage	SEM, XPS, Single fibre tensile test
	2020, Liang, et al. [89]	CFs (Toho Tenax®-E HTA40 E13 6K 400 tex)	at < 32 °C for 2–8 min, 75 Pa, 25% N_2 + 75% H_2 and Ar + N_2 + H_2, 30 mm to side AS cage	SEM, Raman, X-ray diffraction (XRD), Single fibre tensile strength, ILSS and flexural strength
For better catalyst layer grown in subsequent chemical process	2014, Du, et al. [120]	C paper (SIGRACET®, GDL 35BC)	at 120 °C for 10 min, 75% H_2 + 25% N_2, 200 Pa, 15 mm from top AS lid	SEM, TEM, XRD, XPS, CV
	2016, Lin, et al. [121]		at 100–210 °C for 10–30 min, 75% H_2 + 25% N_2, 400 Pa, 15 mm from top AS lid	SEM, CV, Single cell tests
For enhanced electrical properties with ASP-deposited metal nanoparticles	2017, Corujeira Gallo, et al. [122]	CNFs (Sigma-Aldrich, 719811)	at <400 °C for 15–120 min, 75 Pa, 75% H_2 + 25% N_2, 15 mm from top lid, with Ag/Ni target plates	SEM-EDX, TEM, XRD, CV, Cyclic charge-discharge, Electrochemical impedance spectroscopy (EIS)
	2019, Li, et al. [34]	CNFs (Sigma-Aldrich, 719811)	at 320 °C for 6–60 min, 75 Pa, 75% H_2 + 25% Ar, 33 mm from top lid, with Ag/Pt/Pd target plates	SEM-EDX, CV, EIS
For low-temperature reduction, functionalisation and nanoparticle decoration	2015, Chen, et al. [123]	Drop-casted GO film (made via modified Hummer's method)	at 100–200 °C for 1 h, 400 Pa, 100% H_2 and 75% H_2 + 25% N_2, 25 mm from top AS lid	OM, TEM, Ultraviolet-visible spectroscopy, XRD, Raman, Electrical conductivity, XPS
	2020, Jing, et al. [124]	Drop-casted GO film (Sigma-Aldrich 777676)	at 100 °C for 1 h, 75 Pa, 75% H_2 + 25% N_2, 15 mm from top AS lid	SEM-EDX, Raman, XPS, Sheet resistance, CV, EIS, Galvanostatic charge/discharge

[a] Workpieces are under floating potential in all studies.

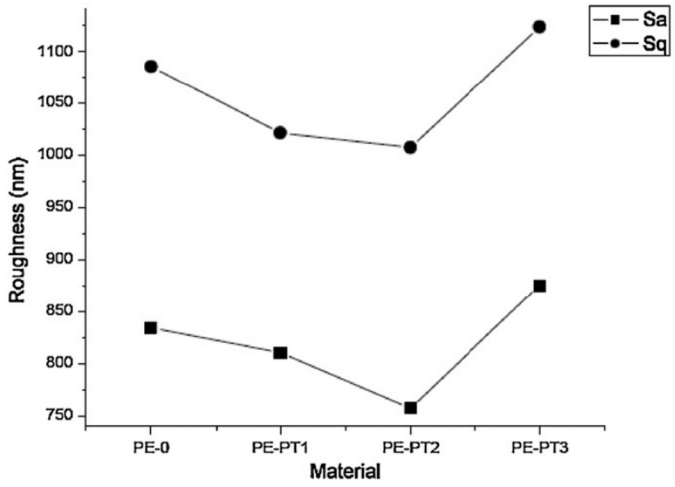

Fig. 2. Showing the change in surface roughness (S_a & S_q) following ASPN treatment of UHMWPE (PE-0) at 120 °C for 10 (PE-PT1), 30 (PE-PT2) and 60 (PE-PT3) min [66].

based treatment layers at relatively higher temperatures (e.g. >300 °C) and/or longer durations (e.g. >5 h). ASP treatments are typically carried out with a gas pressure between 50 and 400 Pa (0.5–4 mbar) [6,23,42]. Gas pressure determines the key gaseous constants (e.g. total number and mean free paths of gas molecules), which influence the negative glow of the glow-discharge plasma within the chamber, in addition to the power transfer density between the anode and the cathode during ASP treatments.

More importantly, it is also possible to adjust the processing conditions at the treated surface by changing the ASP treatment configuration. In close vicinity of the surface to be treated, the level of plasma intensity and the density of sputtered material (that originated from the active-screen) can be adjusted by controlling the distance between the surface and the active-screen. For example, ASP treatments within a typical modified Klöckner DC plasma unit (Fig. 1a) employ distances ranging at 10–30 mm (between sample surface and the top AS lid). Given the perforated mesh structure of the active-screen, treatments tend to become inhomogeneous under small spacing (e.g. < 10 mm, after which outlines of the active-screen holes are observed on the treated surface), while large spacing (e.g. > 20 mm) typically results in lower plasma intensity and 'milder' treatments. In the case of industrial scale active-screen furnaces (Fig. 1b), in lieu of this spacing, a bias power (with low current) can be used to overcome the large distances between sample surfaces and the active-screen and to provide homogeneous treatment coverage [31,38,43]. Additionally, different sputtering targets (typically made of precious metals, as shown in Section 3) can be integrated with the AS to achieve deposition of nanoparticles for surface functionalisation.

Plasma technologies have been extensively adopted for surface modification (for enhanced hardness and wear performance) of ferrous alloys (e.g. austenitic [40,44–49], ferritic [50], martensitic [51,52], and duplex stainless steels [53]), titanium alloys (e.g. Ti6Al4V [36]) and CoCrMo alloys [54]. More recently, for its unique characteristics (predominantly the remote plasma nature and the sputtering-deposition from the active-screen), ASP has been explored for the treatment of biopolymers and carbon-based materials (that have demonstrated promising property enhancements), which forms the theme of this current state overview. In this paper, the recent developments (and impact) of active-screen plasma technologies for the multi-functionalisation of biopolymers and carbon-based materials are introduced and reviewed.

2. Active-screen multi-functionalisation of biopolymers

Polymer materials are widely used within the medical and biomedical industries, as both temporary and permanent solutions, and can be found applied as modules within prosthetic implants [55], as bone cements [56], as scaffolding for tissue engineering [57], as part of drug delivery systems [58,59], and within medical instruments/devices (e.g. urinary catheters) [60,61]. Therefore, modification of polymer materials through surface engineering has widespread potential for the enhancement of performance and expansion of applications. Although there are widespread surface engineering techniques reported for the modification of biopolymers [61–65], in this section we review the recent work carried out within the University of Birmingham on ASP

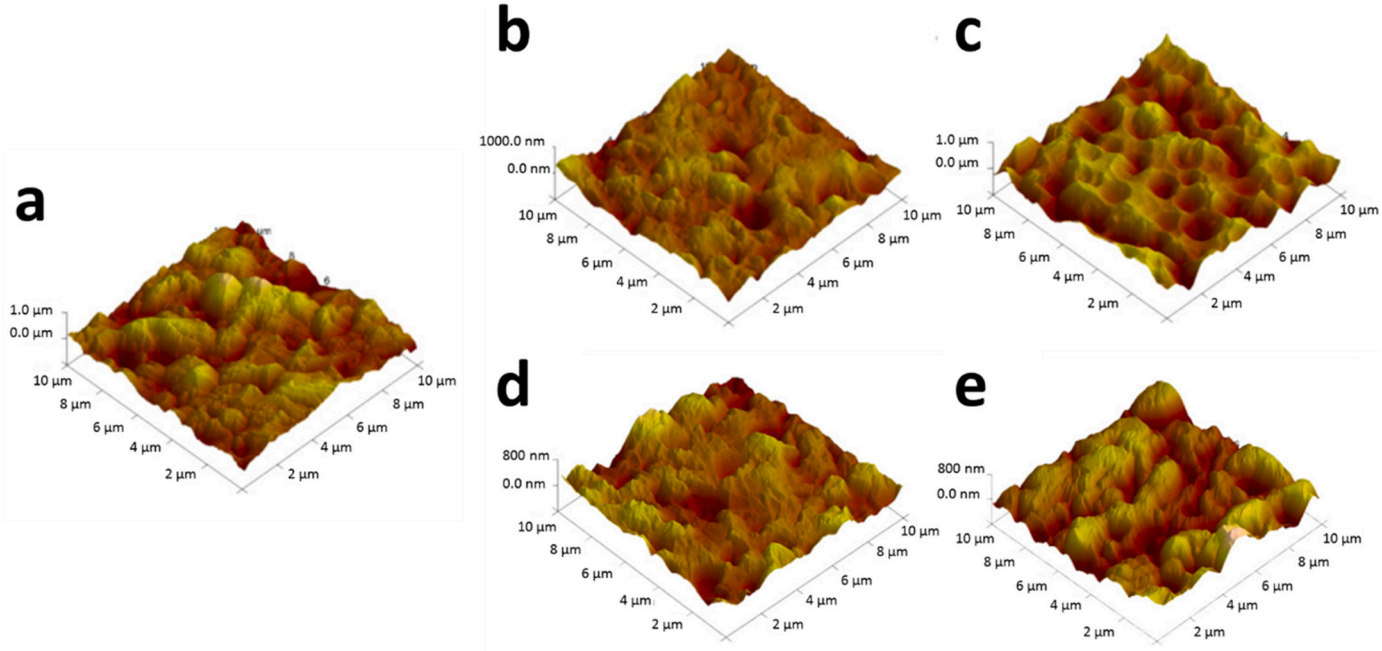

Fig. 3. AFM surface morphology images of polyurethane, a) untreated, b & c) after ASPN at 80 °C and 130 °C for 30 min, respectively, and d & e) after thermal treatment at 80 °C and 130 °C for 30 min, respectively [69].

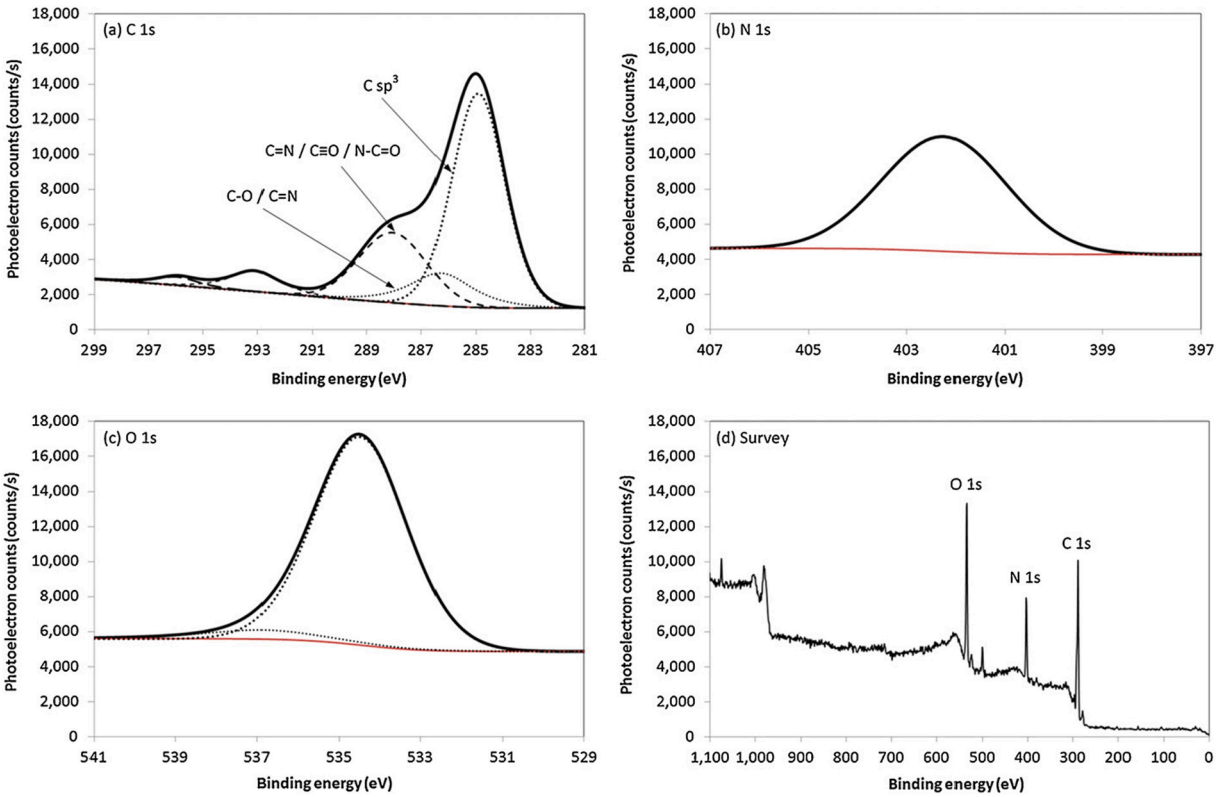

Fig. 4. XPS analysis of UHMWPE treated for 60 min under ASPN conditions, showing deconvoluted peaks of a) C1s, b) N1s and c) O1s, and d) overall XPS survey spectrum of the sample [70].

multi-functionalisation of biopolymers (e.g. polyethylene [66], polytetrafluoroethylene (PTFE) [67], polycaprolactone (PCL) [68], polyurethane [69,70]), where the focus is on the influence of ASP treatments on the surface topography, surface chemistry, wettability and biocompatibility of the polymeric materials (as summarised in Table 1). Typically, for biopolymer treatments, ASP nitriding (ASPN) is employed using varying ratios of nitrogen and hydrogen (with 25% N_2 + 75% H_2 being the most common) [43].

2.1. Effect on surface topography

Given the phenomena of material sputtering from the active-screen, followed by the subsequent deposition onto samples, it would be reasonable to expect an increase in surface roughness following ASP treatment; and indeed, this is a widely reported effect for treatments at high temperatures (e.g. > 300 °C) for prolonged durations (e.g. > 5 h) [73,74]. However, at low temperatures and for short treatment durations where such "sputtering-deposition" material transfer mechanisms are limited, as typically used for polymeric materials, the reported findings have varied [66,69,75,76].

In the study by Kaklamani et al. [66], it was observed that ASPN treatments of ultrahigh molecular weight polyethylene (UHMWPE) at 120 °C initially resulted in the reduction of the measured surface roughness (10 & 30 min treatments), while only the prolonged treatment (for 1 h) gave the expected increase in surface roughness (Fig. 2). However, this finding can potentially be misleading, given the limitation of laser interferometry for measuring the true surface profile of deep and narrow valleys (as found on the treated sample surfaces), thus leading to the impression of surface rounding (or smoothing) and overall reduction of surface roughness following the short plasma treatments. With extended treatment durations, the protruding roughness induced due to the ASP treatment (e.g. from sputtering) begin to outweigh the other measuring limitations, and result in a measured increased in roughness. Similar findings have also been previously reported on the reduction of surface roughness following ASP treatment of polymers [70] and aluminosilicate glasses [71] when using laser interferometry to quantify surface roughness. Additionally, similar trends have also been reported using 2D stylus profilometry of ASP treated polyurethane samples, which can suffer from similar limitations as laser interferometry (depending on the radius of the stylus tip) [69].

In a study by Fu et al. [69], comparisons were made between vacuum thermally treated and ASP treated polyurethane samples, and it was found that no significant difference could be measured between the surfaces of the two treatment types using 2D stylus profilometry. However, this was not the case when using scanning electron microscopy (SEM) imaging to measure the surface topography, which revealed significant modifications of the surface following ASP treatment (in comparison with untreated and those vacuum heat treated surfaces at equivalent temperatures), thereby demonstrating the influence of the ASP treatment on both the surface morphology and condition. SEM and atomic force microscopy (AFM) images of the ASP treated polyurethane surfaces revealed a change in surface roughness with increasing plasma treatment temperature. The sample surfaces were found to change from closed cell structures to porous open structures containing adjacent cracks (Fig. 3). Fu et al. [69] suggested that this was due to the active species within the plasma impinging onto the treated surface, which formed deeper and wider craters/pores. Additionally, by exceeding the T_g (glass transition temperature; 112.5 °C) of the polyurethane during the plasma treatment at 130 °C, the increased mobility of the molecular chains enabled these pores and craters to be formed more readily (Fig. 3c). Further evidence of the influence of the plasma atmosphere was demonstrated by the lack of pore/crack formation following thermal treatment at 130 °C, with surface smoothing being observed instead, which can be attributed to the increased mobility of the polymer chains when exceeding the T_g (Fig. 3e).

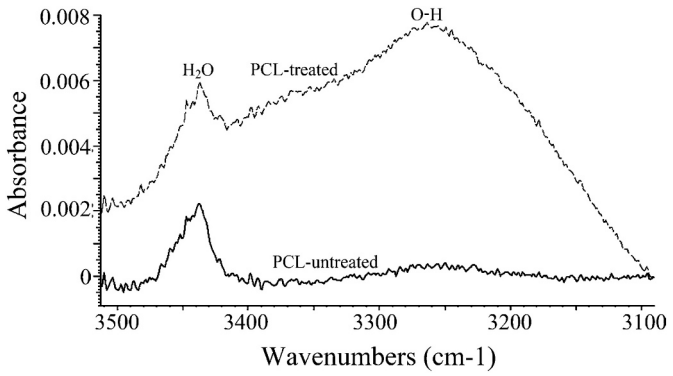

Fig. 5. FTIR spectra of PCL polymers before and after ASPN at 50 °C for 10 min [68].

2.2. Effect on surface chemistry

The reactive and energetic nature of plasma, even at collectively low gas temperatures (e.g. <150 °C), creates opportunities to modify the chemistry of surfaces or to form, in situ, chemical compounds or reactive species (e.g. reactive oxygen species) under mild treatment conditions. Exploitation of this advantage has enabled a multitude of applications, including the treatment and functionalisation of polymer materials [66,68–72], potential future treatments of cancerous cells [77–80], potential enhancement of wound healing [81–85], and treatment of fibres within fibre-reinforced composites [86–89].

ASP treatments have been widely reported to be effective for both the introduction and reorganisation of surface chemistry of polymeric materials. In a study by Kaklamani et al. [70] on the ASPN treatment of UHMWPE, it was found through X-ray photoelectron spectroscopy (XPS) analysis that the overall nitrogen content increased on the treated surfaces. Deconvolution of the XPS spectra at the C1s (285 eV) peak and the shifting of the N1s peak position (from 400 eV to ~402 eV) of the treated surfaces revealed the potential introduction of numerous nitrogen-containing functional groups through the formation of new covalent bonds, such as C—N, C═N, C≡N and C–N–O (Fig. 4). The formation of these nitrogen moieties (functional groups) was explained to be due to the strong reductive nature of the hydrogen plasma found in typical nitriding treatments (75% H_2 + 25% N_2), in combination with the formation of nitrogen species (e.g. primary amides) in the remote plasma (i.e. away from the active-screen) [90,91]. These findings agree with previous reports on ASPN treatment of UHMWPE [66], where the measured nitrogen content and quantity of moieties were also found to increase. This was further confirmed using Fourier-transform infrared spectroscopy (FTIR) data in the study by Kaklamani et al. [66], where the development of N—H stretching and C—N stretching absorption peaks at wavenumbers of 829 cm^{-1} and 1286–1288 cm^{-1}, respectively, were found to have formed after 30 and 60 min ASPN treatment. Similar findings have also been reported for polyurethane [69], where an overall increase in surface nitrogen concentration, increase of existing (or formation of new) nitrogen-containing bonds, and potential formation of cross-linked networks were observed using XPS analysis following ASPN treatment.

The introduction of oxygen and oxygen-containing functional groups is another interesting phenomenon observed following ASPN treatment of polymers. In a study by Fu et al. [68] on the ASPN treatment of PCL, modification of oxygen groups were observed following plasma treatment. Specifically, decomposition of –(C═O)–O–, C–O–C and C═O bonds into hydroxyl containing groups, as well as the development of cross-linking between polymer chains, were identified as potential causes for this change (Fig. 5). According to the findings by Kaklamani et al. [66], the increased presence of oxygen can be explained through the introduction of free radicals onto the treated surfaces, thereby creating 'active' surfaces. The combination of surface activation, with subsequent sample storage and sample transport in air, enabled the post-treatment rapid modification (oxidation) of the surface, including the uptake and formation of oxygen moieties. A recent study [72] on the ASPN treatment of polyhedral oligomeric silsesquioxane combined with poly(carbonate urea) urethane (POSS-PCUU) has also demonstrated the formation of R–C═O bonds (using XPS), as well as the potential formation of –COOH functional groups and NH_2 (suggested by the pH sensitive nature of the treated materials) following ASPN treatment.

2.3. Effect on surface wettability

The most common form of surface wettability assessment is performed using deionised water as the testing liquid. The angle formed between the fixed volume of water used in the test can give insights into the hydrophilicity (< 90°) or hydrophobicity (> 90°) of the surface [92]. Given the mixture of polar (σ^P) and dispersive (σ^D) energies within the surface tension of deionised water (σ^P = 51.00 mN/m; σ^D = 21.8 mN/m), the change in angle formed before and after a surface treatment can give an indication of any alteration in the surface functionality or the surface free energy. It should be noted that surface topography can also play a critical role on the observed contact angle, with different outcomes being arising depending on whether the testing liquid can penetrate surface features (Wenzel state) [93] or air can become trapped within topographical features (Cassie-Baxter state) [48,94,95]. However, significant influence of such phenomena are typically only observed on specifically developed surfaces (e.g. textured surfaces with highly repetitive features). In addition to water contact angle (WCA) measurements, it is also possible to perform more general wettability assessments of surfaces to quantify their polar, dispersive and total surface free energies (sum of polar and dispersive components). This can be performed by measuring the contact angles formed when 2 or more testing liquids (with known surface tensions) are dropped onto the surfaces. Subsequent use of the Fowkes or Owens-Wendt-Rabel-Kaelble models, which are both extensions of the Young's equation and the Good's equation, can then be applied to calculate the surface tension values. Due to its fully dispersive surface free energy (i.e. no polar component), which simplifies the calculations, diiodomethane is typically the most popular wetting liquid used, in conjunction with deionised water, for wettability assessments [92,96].

Given the potential for ASP treatments to both introduce surface functional groups (nitrogen-containing and oxygen-containing moieties) and alter the surface topography of different polymer materials (see Sections 2.1 & 2.2), it is reasonable to expect modification of the surface wettability to also follow. In the study by Mehrban et al. [72], a measured reduction in WCA was found for POSS-PCUU samples after ASP treatments under different gas combinations of air, nitrogen and hydrogen. Moreover, the increased hydrophilicity was maintained, despite changes to the pH levels of the deionised water (achieved using HCl or NaOH additions). Enhanced wettability was also reported by Fu et al. [68], who observed reduced contact angles against both deionised water and ethylene glycol following ASPN treatment of PCL at 50 °C for 10 min. Subsequently, using the measured angles for the two liquids, the total surface free energy of the PCL was also calculated to increase (from 28.76 mN/m to 31.87 mN/m), with the contributions being largely assigned to the increased polar component (increased by 2.80 mN/m). Similar findings were also reported following ASPN treatment of polyurethane samples at 80 °C for 30 min [69]. The increase in surface free energy was attributed to a mixture of functionalisation of the surface (e.g. formation of hydroxyl groups, C—N bonds, C═N bonds and C≡N bonds) and modification of the topography (e.g. formation of open pores). However, under higher temperature conditions (130 °C), a reduction of the total surface free energy was observed (due to possible re-organisation of whole polymer chains). Despite the reduction of the total surface free energy at the higher temperature, the overall ratio of the polar component of the surface free energy was maintained, going

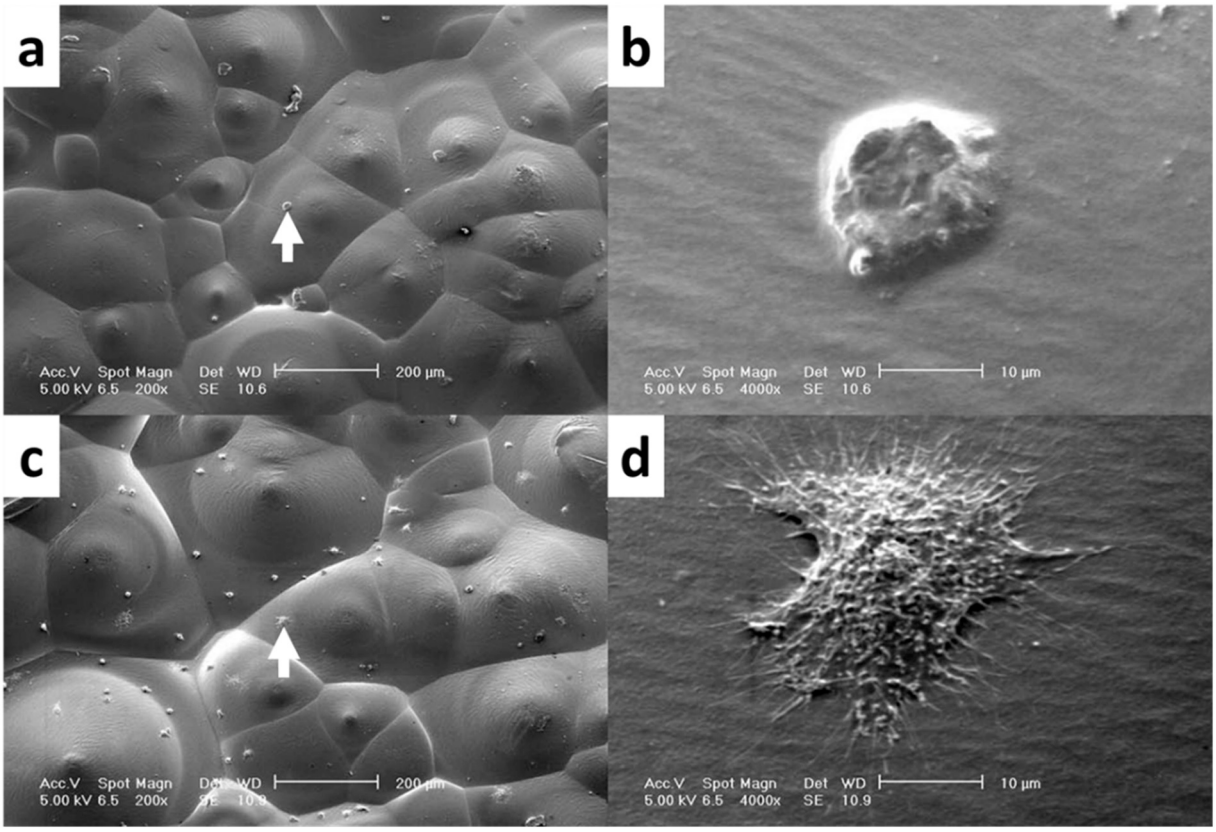

Fig. 6. SEM micrographs of osteoblast-like cell attachment morphology following 1 h contact with a) untreated and b) ASPN treated (at 50 °C for 10 min) PCL surfaces [68]. Images b and d correspond to the magnified regions located at the arrows of images a and c, respectively.

from 15.54% (for the untreated polyurethane) to 96.36% and 94.97% for the 80 °C and 130 °C treated surfaces, respecitvely.

Despite the reported excellent enhancements in surface wettability and increased surface free energy of ASP treated biopolymers, it is widely known that such modified surfaces undergo dynamic changes over time, until relative stabilisation is achieved [48,97,98]. These changes over time are collectively known as the ageing behaviour of the material and can lead to changes (typically tending to return to the untreated state) in the chemical/physical status and biocompatibility of the surfaces (as is described in Section 2.4) [99]. In the case of surface wettability, this is referred to as the hydrophobic recovery, and is commonly attributed to the reorganisation of the hydrophilic polar groups, diffusion of the polymer chains or movement of low molecular weight species from the bulk to the surface, and annihilation of residual radicals (or radicals introduced during ASP treatment) [100–102]. This phenomena was recently demonstrated in a study by Che et al. [21] on the ageing behaviour of glass fibre reinforced polyamide 6 following surface modification using micro-plasma (labelled as µPlasma in the study). It was demonstrated that, across 28 days, large reductions in wettability developed, with rapid hydrophobic recovery arising within the first 5 h, followed by a period of gradual stabilisation in the subsequent weeks. Within the study, the importance of storage conditions (especially relative humidity) to the rate of ageing were also demonstrated, with significantly reduced hydrophobic recovery being reported for micro-plasma treated materials stored under vacuum conditions (in comparison to air storage). Although the concept of material ageing is well known, no direct investigation on the hydrophobic recovery of the biopolymers has been carried out within the studies listed in Table 1. In the future, it would be scientifically valuable to investigate the ageing behaviour of ASP treated biopolymers, as well as methods to preserve the modified surfaces over extended periods of time.

2.4. Effect on biocompatibility

In response to the variety of potential animal cells (e.g. fibroblasts, osteoblasts, immunological cells (e.g. macrophages)), chemical conditions (e.g. pH, proteins), physical conditions (e.g. size, temperature range, flow rates/turbulence) and bacterial cells that can be present within the environment of biomaterials, no surfaces or materials can be regarded as being completely biocompatible [60]. Instead, the response of abiotic materials and/or cells to one another is usually labelled as broad (and ambiguous) levels of biocompatibility, which correspond to the ability of the material to perform its desired function within the biological environment without damage or provoking a local/systemic toxic reaction [103]. Typically, the evaluations of the biocompatibility of materials are measured in differing approaches between studies, with the stages of cell attachment following contact with the surface, degradation of material (e.g. with time) following contact, or potential fouling of the surface being a few of the commonly used approaches for this assessment [60].

With regards to modified surfaces, it is commonly expected that polar surface with increased surface free energies and wettability will induce stronger and more prevalent cell attachment and cell spreading events to arise, which lead to enhanced biocompatibility [104–106]. Given the changes in surface chemistry and wettability (as discussed in Sections 2.2 & 2.3), the improvement of the overall biocompatibility of ASP treated biopolymers are to be expected.

Preliminary studies of the in vitro biocompatibility of ASPN treated UHMWPE with 3T3 fibroblast cells have demonstrated increased (in comparison to untreated counterparts) cell density, confluency (coverage) and proliferation rates following a period of 4 days of incubation at 37 °C [66]. Agreement with these findings has also been demonstrated within the more in-depth analysis of the biocompatibility of UHMWPE with NIH 3T3 fibroblast cells by Kaklamani et al. [70].

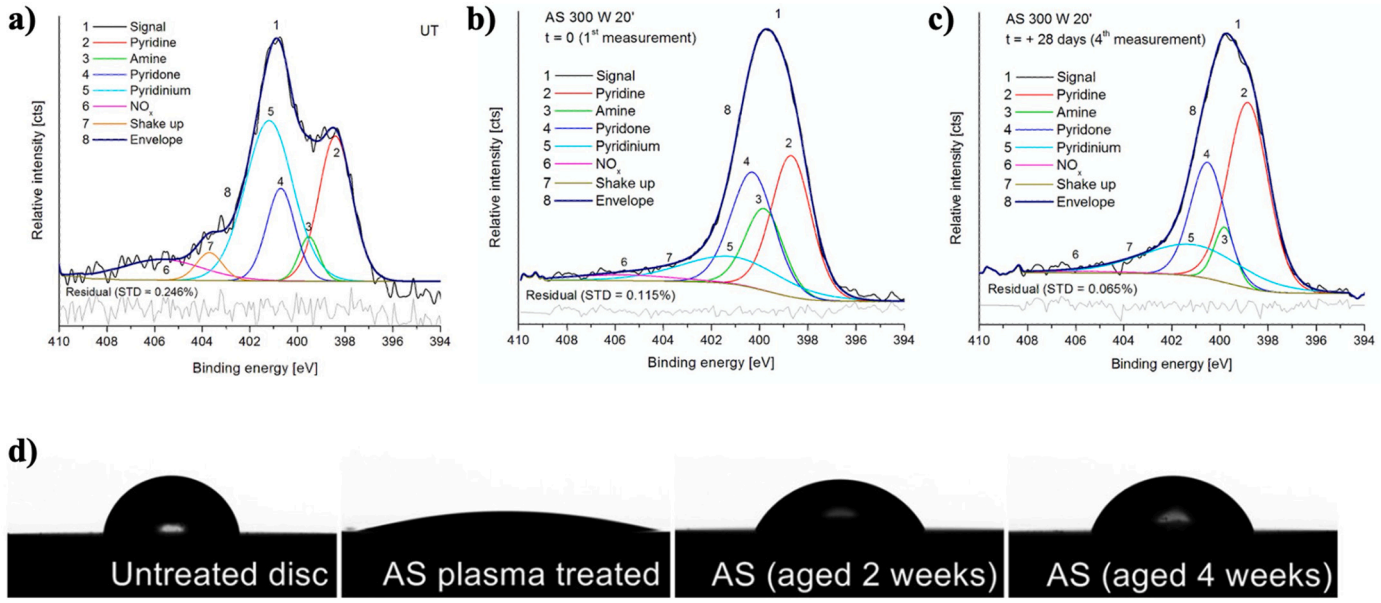

Fig. 7. XPS spectra for N1s peak for a) untreated CFs, b) ASP treated CFs as-treated (at 300 V for 20 min), and c) ASP treated CFs after subsequently ageing in air for 28 days; d) shows the evolution of WCA on vitreous carbon disc, going from left to right: untreated, ASP treated, ASP treated and aged for 2 weeks, and ASP and aged for 4 weeks [118].

Within this study, a significant enhancement of cell attachment, cell coverage, cell flattening, and extracellular matrix excretion was measured after 28-day exposure of the cells on 1 h ASPN treated surfaces. In comparison, no such attachment or flattening could be observed on untreated surfaces. Furthermore, quantification of the number of viable cells presents following 0, 7, 14 and 28 day exposure to the ASPN treated UHMWPE surfaces was analysed using MTT (3-(4,5-Dimethylthiazol-2-yl)-2,5-Diphenyltetrazolium Bromide) metabolic activity assays, which revealed maximum cell activity following 7 days of contact exposure. Although a reduction in fibroblast activity was observed for 14 and 28 day contact periods, the number of cells recorded were still measured to be greater ($\approx 3\times10^6$ cells) than the initially seeded quantity (7.5×10^5 cells). This enhancement after ASPN treatment was explained to be due to the chemical modification of the treated surface, going from an inert surface to a functionalised surface featuring both oxygen- and nitrogen-containing moieties. The introduction of these functional groups is believed to improve the adhesion of glycoproteins (e.g. fibronectin and vitronectin, which typically precede cell attachment), which create the necessary bridge for faster and stronger cell attachment to follow [107–109].

Similar findings have also been reported by Fu et al. [68] on the enhanced in vitro biocompatibility of PCL polymers with mouse MC3T3 osteoblast-like cells following ASPN treatment at 50 °C for 10 min. Within this study, more cells were observed to have anchored onto the PCL surface, and at later stages of cell attachment, as demonstrated by the formation of extended filopodial growth and flattening of cells on the surfaces following 1 h of exposure (as shown in Fig. 6). Moreover, a reduction of the degradation rate of the ASPN treated PCL was also reported during the accelerated degradation testing with PCL (against the enzyme lipase obtained from *Pseudomonas cepacian*). The enhancement

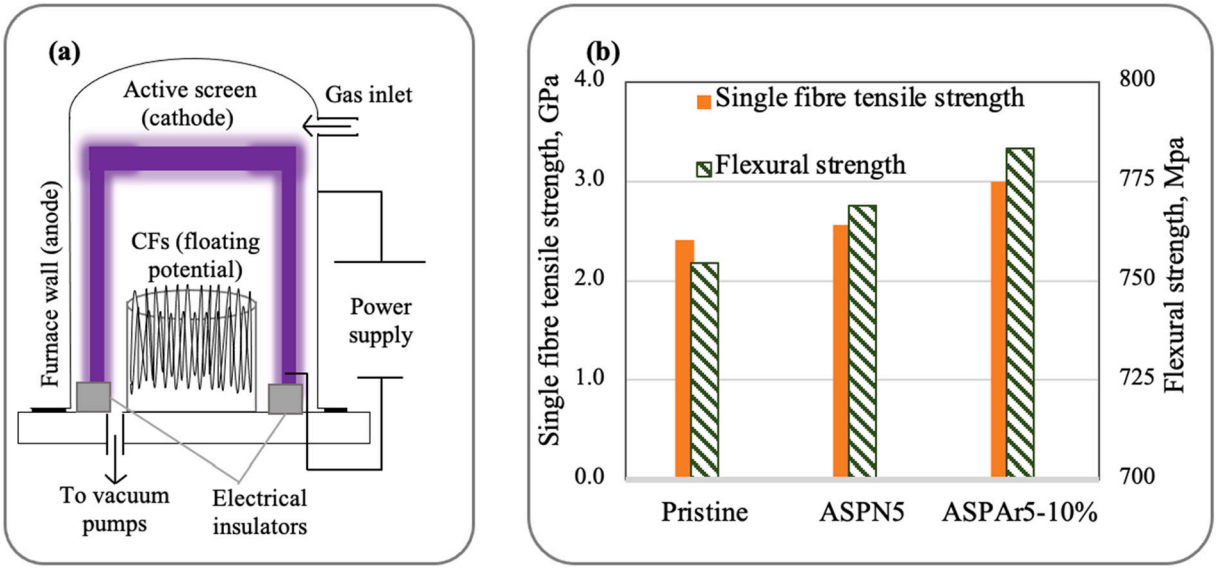

Fig. 8. a) Schematic illustration of ASP treatment for CFs and b) the measured single fibre strength before and after ASP treatments, and flexural strength of the CF/resin composite with CFs before (pristine) and after different ASP treatments (reproduced from Ref. [89]).

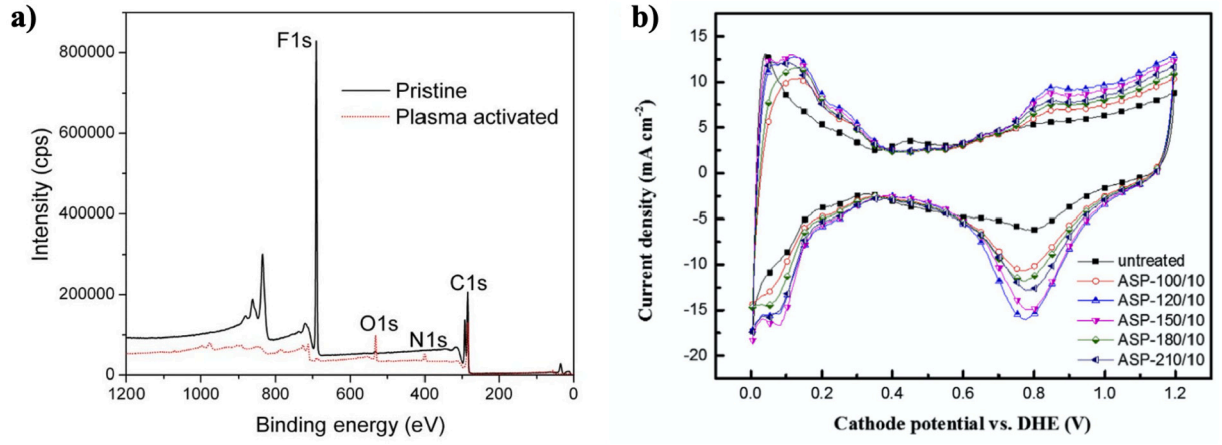

Fig. 9. a) XPS survey spectrum of C paper before (pristine) and after ASP activation, retrieved from Ref. [120]; b) cathode CV for the Pt nanowires synthesised on C papers after 10 min of ASP activation at different treatment temperatures [121].

of the biocompatibility and reduction of the degradation rate were attributed to the improved surface hydrophilicity (enabling more intimate cells-surface interactions to develop) and to the potential cross-linking of the PCL polymer near the surface (as previously described in Section 2.2).

3. ASP functionalisation of carbon-based materials

Carbon-based materials, owing to their vast abundance, thermal stability, good mechanical properties, corrosion resistance and electrochemical properties, have been increasingly studied and implemented in a wide range of applications, ranging from carbon fibres (CFs) for mechanical reinforcement in composites [110] to carbon nanofibres (CNFs) or graphene oxide (GO) for energy conversion and storage devices [111–113]. Further efforts are being made to improve and expand their capabilities, for existing and potential applications, through surface engineering. Firstly, rendered by their chemical inertness, CFs show poor interfacial bonding strength to polymeric matrix materials for composites. This long-standing challenge can be overcome through surface modification of CFs [114]. Secondly, in addition to capabilities for enhancing surface wettability (to electrolytes), carbon-based electrodes can also be activated with "capacitor-like" surface functional groups following surface modification, that contribute to increased "apparent-capacitance" via a "pseudo-capacitor" behaviour for high-performance electric capacitors [115]. CNFs, which have high surface-to-volume ratios, show more pronounced benefits from the addition of functional groups after surface modifications. A great number of studies have already been carried out to functionalise CNFs [116]. Additionally, GO (and reduced GO) – being a promising 2D material for capacitors [117] – can also benefit from surface modifications. ASP, being a versatile and powerful surface engineering technology with good track record for treating metals and polymers, offers great opportunities for surface modification of the abovementioned carbon-based materials. Studies on ASP treatment of carbon-based materials have been carried out and are reviewed in this section (as summarised in Table 2).

3.1. ASP activation of CFs for enhanced wettability and improved bonding to polymer in composite

Plasma – as review by Corujeira Gallo and Dong [25] – is capable for surface modifications of CFs, via the introduction of functional groups, ion bombardment to aid contamination removal, micro-roughening and increasing structural disorder. In 2017, Corujeira Gallo, et al. [118] reported that ASP treated CFs (at <100 °C for 5–40 min in 25% N_2 + 75% H_2), while showing no obvious changes in surface morphology compared to untreated CFs, exhibited significant changes in the shape of the N1s peak and increases in the N content under XPS analysis (Fig. 7a&b), which correlated well to the active species of NH and N_2* in plasma observed using optical emission spectroscopy (OES). Given the difficulties associated with the direct measurement of WCAs of fine CFs (e.g. with fibre diameter of 7 μm), WCAs have been instead measured on ASP treated vitreous C disks, which revealed significantly reduced WCAs, dropping from ~80° (for untreated disks) to as low as ~10° (after ASP treatment at 300 V for 5 min). Investigation on hydrophobic recovery revealed a stabilised WCA at ~70° for ASPN-treated C disks after exposure in air for one week (Fig. 7d) [118].

As reviewed by Sharma et al. [114], most surface treatments for CFs (such as conventional LPP, acid, γ-ray, etc.) show increased structural disorder ratio (i.e. I_D/I_G) and decreased surface crystallite size (La), which can be translated to the distortion of the graphitic structure [125]. The interfacial bonding of CFs to resins is often improved at the cost of reduced single fibre tensile strength using conventional LPP [126,127]. However, Liang, et al. [89] reported that, compared with untreated CFs, ASP treated CFs were observed to have decreased I_D/I_G ratios with increased crystallite sizes. It was demonstrated that short ASP treatments (of the order of ~2–5 min) can improve the interfacial bonding of CFs to epoxy resins with no reduction of, and in some cases improvement of, single fibre tensile strength (Fig. 8b). This finding can be attributed to the remote plasma nature of the treatment, thus limiting ion bombardment (and subsequent material damage/degradation) as a result of the floating potential conditions, and large spacing (i.e. 30 mm) to the active-screen, employed during ASP treatments (Fig. 8a) [89]. Similarly, in a separate study by Semitekolos et al. [119], the single fibre tensile strength of CFs was measured to drop by 10–15% after conventional LPP treatments (for 5 min at 20–40 Pa in O_2 atmosphere). Whereas, the single fibre tensile strength of CFs increased after ASP treatments, leading to significantly improved (by 11–16%) bending strength for the following CF-reinforced polymer composite. Additionally, the wettability of ASP-treated CFs was evaluated using the contact angles formed between resin droplets and single CFs, where the resin contact angle was shown to reduce from ~70.6° for pristine CF to ~57–61° for CFs after short (2–8 min) ASP treatments. Comparing the resin contact angles for day 1 and day 10 after ASP treatment, hydrophobic recovery between 0.62 and 5.04% was reported [128].

3.2. ASP activation of C paper to promote the growth of Pt nanowires

In 2014, Du et al. [120] demonstrated that short (10 min) ASP treatment at 120 °C can be used to activate the surface of commercial C paper for vertically growing 2.5–3 nm diameter Pt nanowires (during a subsequent wet chemical process) to obtain large and high-performance catalyst electrodes, which outperformed a conventional Pt nanoparticle

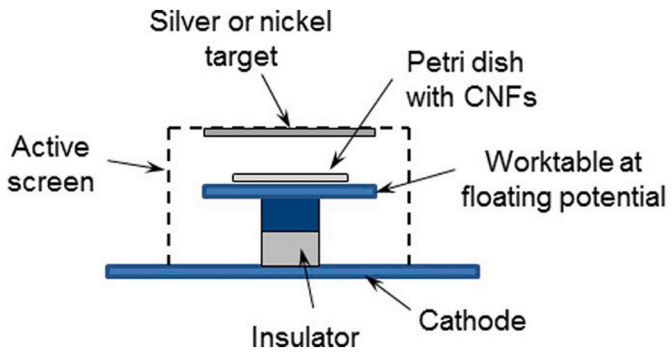

Fig. 10. Experimental setup for ASP-deposition treatments of CNFs [122].

cathode under cyclic voltammetry (CV) testing in a direct methanol fuel cell. Both the introduction of functional groups (such as C—N, C═N, and –OH) and N-doping during the ASP treatment were revealed under XPS, which was believed to have promoted the formation of uniform Pt nuclei in the subsequent chemical growth process [120]. Additionally, comparing the XPS profiles of pristine and ASP treated C paper, the absence of F1s peak (for C—F) and C1s peak (for C—F_2) following ASP treatment indicated the removal of the hydrophobic PTFE film on pristine C paper [120], that also contributed to promoting the growth of uniform Pt nanowires (Fig. 9a).

In 2016, Lin, et al. [121] systematically explored the influence of treatment temperature and time (at 100–210 °C for 10–30 min) on the electrical properties of the following catalyst layer grown, attempting to optimise ASP treatment conditions. The improvement in electrical properties after ASP treatment was evident from the CV shown in Fig. 9b. The specific power density at 0.4 V was found to be at the highest (at 63.9 mW/cm^2) for the samples after ASP treatment at 120 °C for 10 min, compared to those without ASP activation (at 18.2 mW/cm^2), and to those at other ASP treatment conditions (ranging between 15.2 and 52 mW/cm^2). Further increases in ASP treatment temperature (above 120 °C) and duration (above 10 min) resulted in a "disproportionate decline" of power density, that could be associated to the development of large pores after ASP treatment and/or the comparatively shorter Pt nanowire grown during subsequent wet chemical process [121].

3.3. ASP-deposition on CNFs for improved electrical properties

Apart from enabling surface modification at floating potential, ASP-deposition of metallic nanoparticles (NPs) via the "sputtering-deposition" mechanism [28,29,32,38] can also be exploited in surface treatments through the integration of metallic sputtering targets to the ASP configuration (e.g. Ti and Cu metal plate lids, which can be traced back to a study in 2002 by Li et al. [29]). In 2017, Corujeira Gallo et al. [122] explored the feasibility of functionalising CNFs with Ag and Ni nanoparticles under ASP treatment in 25% N_2 + 75% H_2 at 75 Pa, where Ag or Ni target plates were attached at the top of the AS cage (Fig. 10). Formation of nanoparticles on the surfaces were observed under both SEM and transmission electron microscopy (TEM), as shown in Fig. 11. Both ASP-deposited Ag and Ni NPs showed increasing particle size with increasing treatment duration (15–120 min), which correlated strongly with the increasingly larger loop areas observed under CV curves. While enhanced electrical capacitance was observed on CNFs after ASP deposition with both Ag and Ni NPs, those CNFs after ASP-Ag treatment

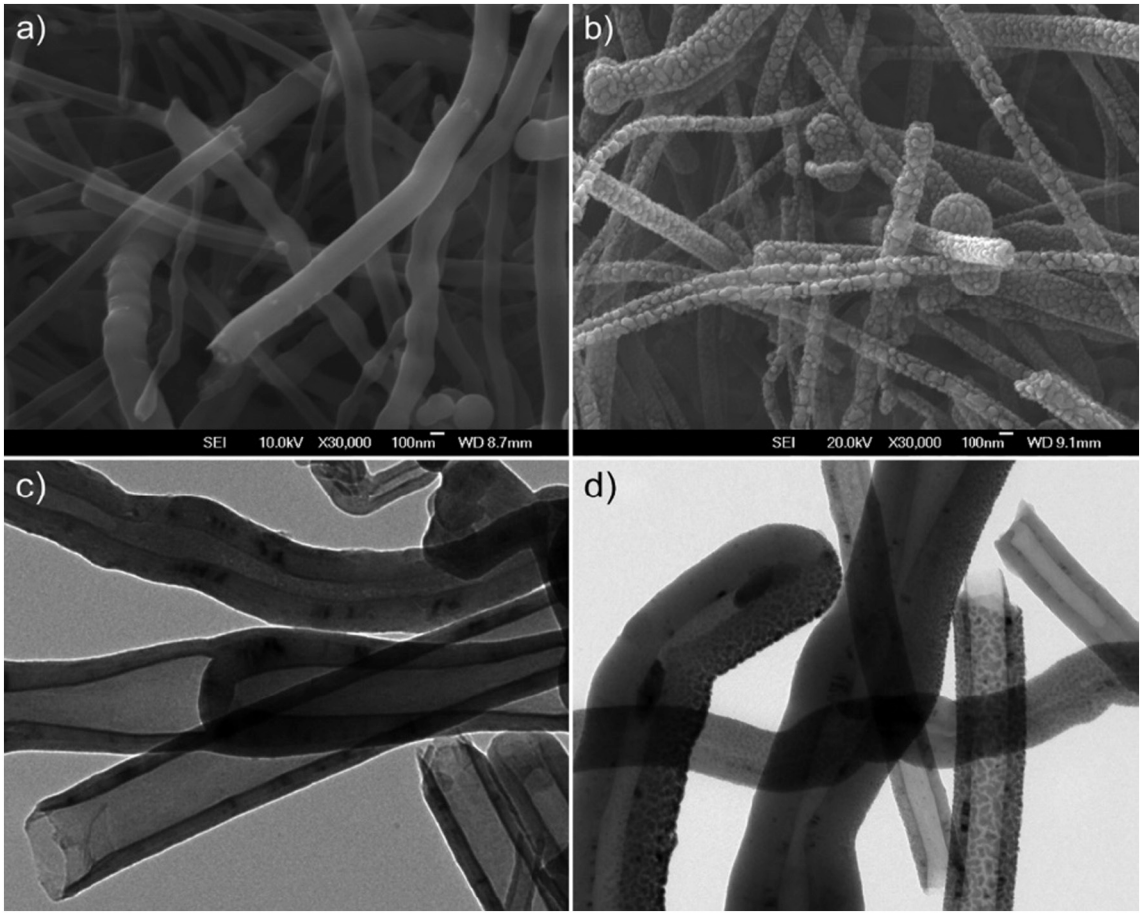

Fig. 11. SEM and TEM images for CNFs a, c) before and b, d) after ASP-Ni treatment [122].

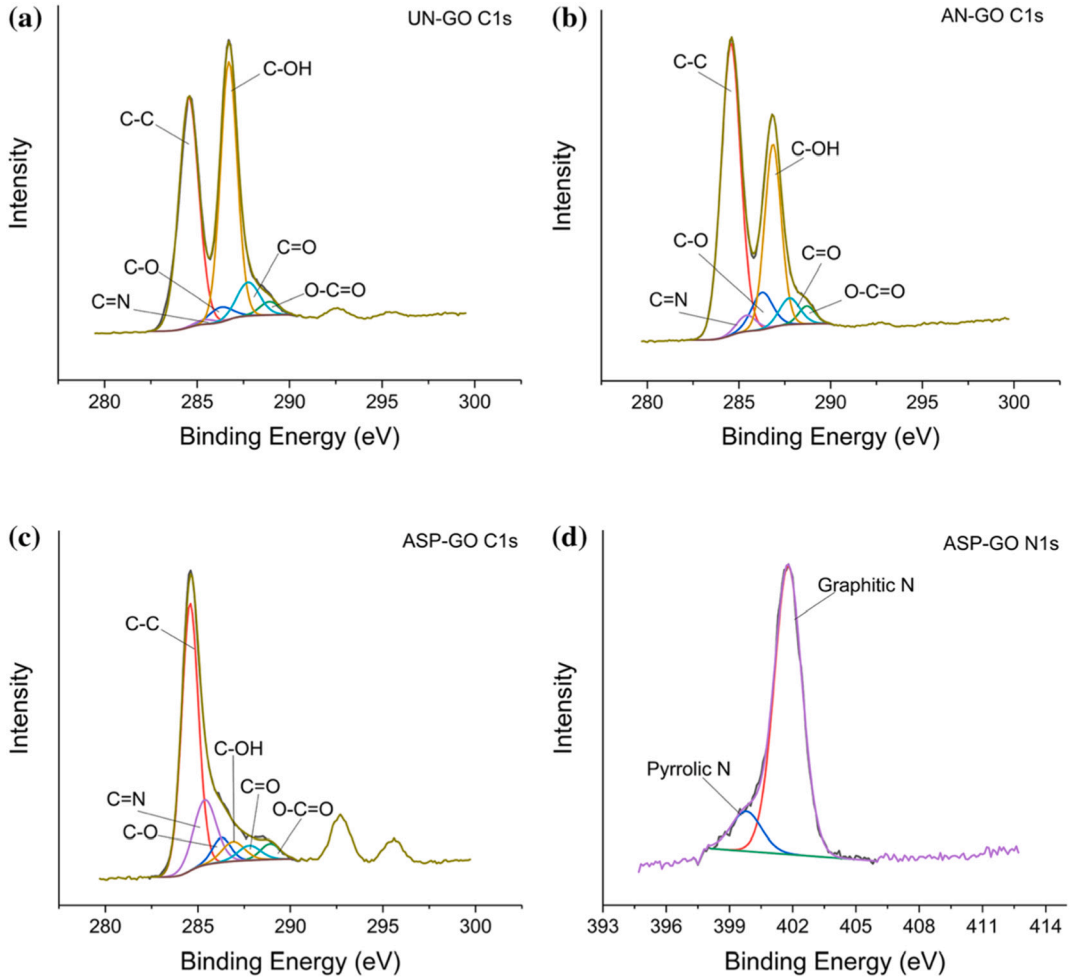

Fig. 12. High-resolution XPS spectra showing C1s peak for a) untreated GO, b) thermally annealed GO, c) ASP treated GO and d) N1s peak for ASP treated GO [124].

demonstrated much greater capacitance enhancement in comparison with those after ASP-Ni treatments [122]. It is also worth mentioning that poor deposition uniformity and coverage was observed [122], that may require further improvement in the future.

Under similar ASP treatment conditions, Li et al. [34] explored surface modification of CNFs with Ag, Pd and Pt particles at ~320 °C for 6–60 min, where ASP treated CNFs were found to exhibit different levels of enhancement in electrical capacitance. The scan-rate-dependent enhancements in electrical capacitance were discussed with respect to the different types of porous structures obtained (i.e. macropores at >50 nm, mesopores at 2–50 nm and nanopores <2 nm) on surfaces after ASP-Ag/Pd/Pt treatments. Although the highest capacitance (at 10.5 F/g) was seen for those CNFs with Pt NPs, the ASP-Pt treated CNFs showed a poor rate capacity. While Ag and Pd nanoparticles were found to agglomerate (increase in size) with ASP treatment time, ASP-deposited Pt NPs, showed a constant fine distribution at all three treatment durations employed in the study (i.e. 6, 12 and 30 min) [34]. The fine ASP-deposited Pt NPs appear to pile up evenly on the CNFs with increasing treatment duration, forming a smooth final surface finish. It was argued that the lack of mesopores for fast ion diffusion on the smooth ASP-Pt modified surfaces limited the formation of the electrochemical double layer, resulting in poor rate capacitance. It was also found that ASP-Ag treated CNFs presented the best life-cycle performance. After 2000 charge/discharge cycles, in comparison to the 15–17% reduction in electrical capacitance for the ASP-Pt/Pd treated CNFs, those CNFs after ASP-Ag treatments showed no significant drop in capacitance.

3.4. Multipurpose ASP treatment of GO films for enhanced electric and electrochemical properties

In 2015, Chen et al. [123] characterised and compared drop-casted GO films (on polyethylene terephthalate substrates) after thermal annealing (in pure H_2) and after ASP treatments (in pure H_2 and in a gas mixture of $H_2 + N_2$) at 100–200 °C. In addition to the changes in colour, going from a light brown (as drop-casted) to a silver-grey (after ASP), ASP treatments also acted to simultaneously reduce the GO, dope the GO surface with N (from the nitrogen-rich atmosphere) and deposit the GO surface with metallic species (from the active-screen) [123]. The electrical resistance of ASP treated GO was found to reduce with increasing treatment temperature [123]. However, compared with thermally annealed GO at equivalent treatment conditions, ASP treatments induced greater enhancement in electrical conductivity for GO films (more significant at the lower treatment temperature of 150 °C than those at 200 °C) [123]. Moreover, ASP treatments in $N_2 + H_2$ gas mixtures were always found to provide better enhancements in electrical conductivity than those in pure H_2 (when other treatment conditions were kept the same), which can be associated to the higher efficiency in "multi-element doping" provided by the additional N_2 in the gas mixture [123].

In 2020, Jing et al. [124] further investigated the enhanced electrochemical properties for drop-casted GO films (on Si wafer substrates) after ASP treatment in 25% N_2 + 75% H_2 at 100 °C, which were also compared to thermally annealed GO films (at 100 °C in pure Ar). Compared to thermal annealing, ASP offered a multi-functional

treatment with combined GO reduction, N doping and deposition of metal NPs on GO films [124]. Significantly improved electrical conductivity was also measured after ASP treatment, with sheet resistance being reduced from $5.2 \times 10^6\ \Omega sq^{-1}$ as drop-casted to $1.1 \times 10^6\ \Omega sq^{-1}$ after ASP treatment [124]. This change can be attributed to the reduction of the GO, combined with the introduction of graphitic N (which may work as an electron doner during the charge/discharge process [129]) and the absence of pyridinic N (Fig. 12). In agreement with the minor concentrations of Fe, Mn and Cr detected with XPS measurements after ASP treatment, fine (< 10 nm) metal NPs were observed on the surfaces of the GO films. The idea was put forward that the decoration of metal NPs could also have contributed to the good capacitive performance of the ASP treated GO.

4. Summary and concluding remarks

4.1. Summary and conclusions

In summary, the advanced ASP technology has been developed and examined for multi-functionalising biopolymers and carbon-based materials, which possess low electrical conductivity and/or are vulnerable to surface degradation.

The biocompatibility of biopolymers has been shown to be effectively enhanced by low-temperature active-screen plasma activation and functionalisation through the adequate modification of surface morphology, introduction of desirable functional groups and improvement of surface wettability. This has shown potential for generating strong fixation on polymeric implants, rapid growth of cells on polymeric scaffolds for tissue engineering and the adsorption of functional peptides onto implantable polymers.

Enhanced interfacial shear strength between carbon fibres and the polymeric matrix has been achieved through active-screen plasma activation and functionalisation. Due to the remote plasma nature, the single fibre tensile strength of the CFs has been demonstrated to increase after ASP treatment, rather than decrease (as is the case for many other plasma treatment techniques). These achievements could pave the way towards future carbon fibre reinforced high-performance and long-life composites for aerospace, automotive and wind energy applications.

The unique combined function of surface activation and deposition (CFAD) of nanoparticles using the advanced ASP technology has shown great potential for improving the electrochemical response of CNFs and GOs. Significantly improved cyclic voltammetry performance and specific capacitance have been achieved on CNFs through the additions of Ag, Pd and Pt nanoparticles by the CFAD mechanism of the ASP technology, while the ASP multi-functionalisation of GO has shown significantly improved electrical properties and effectively enhanced supercapacitive performance as a consequence of reduction, nitrogen doping and metal/metal oxides NP decoration of GOs.

4.2. Challenges and future directions

As with any technology, it is not possible to satisfy every requirement or scenario, and the three main drawbacks of ASP treatments are: (1) accurate control of the amount and size of the deposited nanoparticles is challenging, (2) it is difficult to treat a large amount fibres continuously due to the batch treatment nature, as is the case for most LPP techniques, and (3) some “line of sight” issues can be developed with complex workpiece geometries under floating potential conditions [130].

The future development of ASP multi-functionalisation of materials with poor electrical conductivity and/or vulnerability to degradation will have the following principle directions: (1) investigation of the time-dependent behavioural changes (e.g. wettability or chemical functionality) of ASP treated biopolymers and carbon-based materials across both short (e.g. <1 day) and prolonged (e.g. 28 days) periods of time, post-treatment; (2) development of continuous treatment techniques for long fibres through the design of roll-to-roll mechanisms within low-pressure ASP chambers; (3) improvement of the control of surface activation and deposition through the incorporation of additional power source within ASP treatments (i.e. triple-glow plasma technologies [131]), enabling multiple simultaneous glow-discharges, and thus rendering extra dimensions of adjustment and more accurate control on plasma intensity and nanoparticles deposition; (4) extending the research to other materials with poor electrical conductivity and/or high sensitivity to surface degradation such as glass fibres and bioceramics; and (5) further explorations of the interactions of ASP treated biopolymers and carbon-based materials to biotic matter, including the antimicrobial activity and biocompatibility assessment of ASP treated biopolymers, and the potential for engineering antibacterial CF reinforced composites through CFAD of Ag nanoparticles.

Declaration of competing interest

The authors declare that they have no known competing financial interests or personal relationships that could have appeared to influence the work reported in this paper.

Acknowledgement

The authors would like to acknowledge the financial support from Smart Factory Hub (European Structural and Investment Funds 06R1702266), SMARTFAN (Horizon 2020 EC760779) and Carbo4-Power (Horizon Europe EC953192) projects.

References

[1] M. Capitelli, C. Gorse, Plasma Technology Fundamentals and Applications, First ed., Springer Science & Business Media, New York, 1992.
[2] J.G. Krüger, Geschichte der Erde in den allerältesten Zeiten, Lüderwald, 1746.
[3] J. Priestley, The History and Present State of Electricity with Original Experiments, J, Dodsley, J. Johnson, B. Davenport, and T. Cadell, 1775.
[4] G. Gilbert, De magnete, magneticisque corporibus, et de magno magnete tellure; Physiologia nova, plurimis & argumentis, & experimentis demonstrata, Petrus Short, 1967.
[5] A. Anders, Tracking down the origin of arc plasma science I. Early pulsed and oscillating discharges, IEEE Trans. Plasma Sci. 31 (2003) 1052–1059.
[6] A. Fridman, L.A. Kennedy, Plasma Physics and Engineering, First ed., Taylor & Francis Routledge, New York, 2004.
[7] M.A. Lieberman, A.J. Lichtenberg, Principles of Plasma Discharges and Materials Processing, Second ed., John Wiley & Sons, Inc, New Jersey, 2005.
[8] D. Staack, B. Farouk, A. Gutsol, A. Fridman, Characterization of a dc atmospheric pressure normal glow discharge, Plasma Sources Sci. Technol. 14 (2005) 700–711.
[9] D. Staack, B. Farouk, A. Gutsol, A. Fridman, DC normal glow discharges in atmospheric pressure atomic and molecular gases, Plasma Sources Sci. Technol. 17 (2008), 025013.
[10] M. Goldman, A. Goldman, R.S. Sigmond, The corona discharge, its properties and specific uses, Pure Appl. Chem. 57 (1985) 1353–1362.
[11] U. Kogelschatz, B. Eliasson, W.A. Egli, Dielectric-Barrier Discharges. Principle and Applications, J. Phys., IV, 07 (1997).
[12] H.E. Wagner, R. Brandenburg, K.V. Kozlov, A. Sonnenfeld, P. Michel, J.F. Behnke, The barrier discharge: basic properties and applications to surface treatment, Vacuum 71 (2003) 417–436.
[13] U. Kogelschatz, Dielectric-barrier discharges: their history, discharge physics, and industrial applications, Plasma Chem. Plasma Process. 23 (2003) 1–46.
[14] R. Brandenburg, Dielectric barrier discharges: process on plasma sources and on the understanding of regimes and single filaments, Plasma Sources Sci. Technol. 26 (2017), 053001.
[15] M. Šimor, J. Ráhel', P. Vojtek, M. Černák, A. Brablec, Atmospheric-pressure diffuse coplanar surface discharge for surface treatments, Appl. Phys. Lett. 81 (2002) 2716–2718.
[16] M. Černák, L. Černáková, I. Hudec, D. Kováčik, A. Zahoranová, Diffuse Coplanar Surface Barrier Discharge and its applications for in-line processing of low-added-value materials, EPJ Appl. Phys. 47 (2009) 22806.
[17] K.G. Kostov, T.M.C. Nishime, A.H.R. Castro, A. Toth, L.R.O. Hein, Surface modification of polymeric materials by cold atmospheric plasma jet, Appl. Surf. Sci. 314 (2014) 367–375.
[18] F. Fanelli, F. Fracassi, Atmospheric pressure non-equilibrium plasma jet technology: general features, specificities and applications in surface processing of materials, Surf. Coat. Technol. 322 (2017) 174–201.
[19] L. Lin, Q. Wang, Microplasma: a new generation of technology for functional nanomaterial synthesis, Plasma Chem. Plasma Process. 35 (2015) 925–962.
[20] W. Chiang, D. Mariotti, R.M. Sankaran, J.G. Eden, K. Ostrikov, Microplasmas for advanced materials and devices, Adv. Mater. 32 (2020) 1905508.

[21] C. Che, B. Dashtbozorg, X. Li, H. Dong, M. Jenkins, Effect of μPlasma modification on the wettability and the ageing behaviour of glass fibre reinforced polyamide 6 (GFPA6), Materials 14 (2021) 7721.
[22] K.S.S. Harsha, Principles of Vapor Deposition of Thin Films, First ed., Elsevier Science, Online, 2005.
[23] D. Pye, Practical nitriding and ferritic nitrocarburizing, ASM International, United States, 2003.
[24] A. Fridman, Plasma Chemistry, Cambridge University Press, Cambridge, 2008.
[25] S. Corujeira Gallo, H. Dong, Effect of microstructure on the plasma surface treatment of carbon fibres, J. Compos. Mater. 51 (2016) 3239–3256.
[26] J. Georges, Nitriding process and nitriding furnace therefor, US5989363A, 1999.
[27] S. Corujeira Gallo, H. Dong, Corrosion behaviour of direct current and active screen plasma carburised AISI 316 stainless steel in boiling sulphuric acid solutions, Corros. Eng. Sci. Technol. 46 (2011) 8–16.
[28] C. Zhao, C.X. Li, H. Dong, T. Bell, Study on the active screen plasma nitriding and its nitriding mechanism, Surface & Coatings Technology 201 (2006) 2320–2325.
[29] C.X. Li, T. Bell, H. Dong, A study of active screen plasma nitriding, Surf. Eng. 18 (2002) 174–181.
[30] C. Li, T. Bell, Corrosion properties of active screen plasma nitrided 316 austenitic stainless steel, Corros. Sci. 46 (2004) 1527–1547.
[31] A. Nishimoto, K. Nagatsuka, R. Narita, H. Nii, K. Akamatsu, Effect of the distance between screen and sample on active screen plasma nitriding properties, Surf. Coat. Technol. 205 (2010) S365–S368.
[32] S. Corujeira Gallo, H. Dong, On the fundamental mechanisms of active screen plasma nitriding, Vacuum 84 (2009) 321–325.
[33] K. Lin, X. Li, L. Tian, H. Dong, Active screen plasma surface co-alloying treatments of 316 stainless steel with nitrogen and silver for fuel cell bipolar plates, Surf. Coat. Technol. 283 (2015) 122–128.
[34] Z. Li, S. Qi, Y. Liang, Z. Zhang, X. Li, H. Dong, Plasma surface functionalization of carbon nanofibres with silver, palladium and platinum nanoparticles for cost-effective and high-performance supercapacitors, Micromachines 10 (2019) 2.
[35] D. Kovács, J. Dobránszky, A. Bonyár, Effect of different active screen hole sizes on the surface characteristic of plasma nitrided steel, Results Phys. 12 (2019) 1311–1318.
[36] A. Nishimoto, K. Nakazawa, Active screen plasma nitriding of titanium alloy using titanium double screen, Mater. Sci. Forum 891 (2017) 11–17.
[37] I. Burlacov, S. Hamann, H.-J. Spies, A. Dalke, J. Röpcke, H. Biermann, A novel approach of plasma nitrocarburizing using a solid carbon active screen – a proof of concept, HTM - J. Heat Treat. Mater. 72 (2017) 254–259.
[38] K. Lin, X. Li, H. Dong, P. Guo, D. Gu, Nitrogen mass transfer and surface layer formation during the active screen plasma nitriding of austenitic stainless steels, Vacuum 148 (2018) 224–229.
[39] M.F. McGuire, Stainless Steels for Design Engineers, ASM International, Materials Park, OH, 2008.
[40] H. Dong, S-phase surface engineering of Fe-Cr, Co-Cr and Ni-Cr alloys, Int. Mater. Rev. 55 (2010) 65–98.
[41] E.J. Mittemeijer, M.A. Somers, Thermochemical Surface Engineering of Steels: Improving Materials Performance, Elsevier, 2014.
[42] A. Nishimoto, K. Nagatsuka, R. Narita, H. Nii, K. Akamatsu, Effect of gas pressure on active screen plasma nitriding response, 18th International Federation for Heat Treatment and Surface Engineering, STP153220120023 (2012) 327–335.
[43] C. Li, Active screen plasma nitriding–an overview, Surf. Eng. 26 (2010) 135–141.
[44] X. Tao, X. Liu, A. Matthews, A. Leyland, The influence of stacking fault energy on plasticity mechanisms in triode-plasma nitrided austenitic stainless steels: implications for the structure and stability of nitrogen-expanded austenite, Acta Mater. 164 (2019) 60–75.
[45] X. Tao, A. Matthews, A. Leyland, On the nitrogen-induced lattice expansion of a non-stainless austenitic steel, Invar 36®, under triode plasma nitriding, Metall. Mater. Trans. A 51 (2020) 436–447.
[46] B. Dashtbozorg, X. Li, J.M. Romano, A. Garcia–Giron, R.L. Sammons, S. Dimov, H. Dong, A study on the effect of ultrashort pulsed laser texturing on the microstructure and properties of metastable S phase layer formed on AISI 316L surfaces, Appl. Surf. Sci., 511 (2020) 145557.
[47] X. Tao, J. Qi, M. Rainforth, A. Matthews, A. Leyland, On the interstitial induced lattice inhomogeneities in nitrogen-expanded austenite, Scr. Mater. 185 (2020) 146–151.
[48] B. Dashtbozorg, P. Penchev, J.-M. Romano, X. Li, R.L. Sammons, S. Dimov, H. Dong, Development of surfaces with antibacterial durability through combined S phase plasma hardening and athermal femtosecond laser texturing, Appl. Surf. Sci. 565 (2021), 150594.
[49] X. Tao, X. Li, H. Dong, A. Matthews, A. Leyland, Evaluation of the sliding wear and corrosion performance of triode-plasma nitrided Fe-17Cr-20Mn-0.5N high-manganese and Fe-19Cr-35Ni-1.2Si high-nickel austenitic stainless steels, Surf. Coat. Technol. 409 (2021), 126890.
[50] R.R.M.d. Sousa, F.O.d. Araújo, J.A.P.d. Costa, A.M.d. Oliveira, M.S. Melo, C. Alves Junior, Cathodic cage nitriding of AISI 409 ferritic stainless steel with the addition of CH4, Mater. Res., 15 (2012) 260–265.
[51] M. Libório, G. Praxedes, L. Lima, I. Nascimento, R. Sousa, M. Naeem, T. Costa, S. Alves, J. Iqbal, Surface modification of M2 steel by combination of cathodic cage plasma deposition and magnetron sputtered MoS2-TiN multilayer coatings, Surf. Coat. Technol. 384 (2020), 125327.
[52] Y. Li, Y. He, J. Xiu, W. Wang, Y. Zhu, B. Hu, Wear and corrosion properties of AISI 420 martensitic stainless steel treated by active screen plasma nitriding, Surf. Coat. Technol. 329 (2017) 184–192.
[53] G. Pintaude, A.C. Rovani, J.C.K. das Neves, L.E. Lagoeiro, X. Li, H.S. Dong, Wear and corrosion resistances of active screen plasma-nitrided duplex stainless steels, J. Mater. Eng. Perform., 28 (2019) 3673–3682.
[54] Y. Dong, P. Svoboda, M. Vrbka, D. Kostal, F. Urban, J. Cizek, P. Roupcova, H. Dong, I. Krupka, M. Hartl, Towards near-permanent CoCrMo prosthesis surface by combining micro-texturing and low temperature plasma carburising, J. Mech. Behav. Biomed. Mater. 55 (2016) 215–227.
[55] S. Ge, S. Wang, X. Huang, Increasing the wear resistance of UHMWPE acetabular cups by adding natural biocompatible particles, Wear 267 (2009) 770–776.
[56] S.B. Kim, Y.J. Kim, T.L. Yoon, S.A. Park, I.H. Cho, E.J. Kim, I.A. Kim, J.-W. Shin, The characteristics of a hydroxyapatite–chitosan–PMMA bone cement, Biomaterials 25 (2004) 5715–5723.
[57] H. Nosrati, K. Ashrafi-Dehkordi, Z. Alizadeh, S. Sanami, M. Banitalebi-Dehkordi, Biopolymer-based scaffolds for corneal stromal regeneration: a review, Polym. Med. 50 (2020) 57–64.
[58] I.R. Calori, G. Braga, P.d.C.C. de Jesus, H. Bi, A.C. Tedesco, Polymer scaffolds as drug delivery systems, Eur. Polym. J., 129 (2020) 109621.
[59] X. Tong, W. Pan, T. Su, M. Zhang, W. Dong, X. Qi, Recent advances in natural polymer-based drug delivery systems, React. Funct. Polym. 148 (2020), 104501.
[60] B.D. Ratner, A.S. Hoffman, F.J. Schoen, J.E. Lemons, Biomaterials Science: An Introduction to Materials in Medicine, Elsevier, 2004.
[61] S.P. Nikam, P. Chen, K. Nettleton, Y.-H. Hsu, M.L. Becker, Zwitterion surface-functionalized thermoplastic polyurethane for antifouling catheter applications, Biomacromolecules 21 (2020) 2714–2725.
[62] A. Manteghi, S. Ahmadi, H. Arabi, Enhanced thermo-oxidative stability through covalent attachment of hindered phenolic antioxidant on surface functionalized polypropylene, Polymer 138 (2018) 41–48.
[63] R. Liu, J. Zhao, Q. Han, X. Hu, D. Wang, X. Zhang, P. Yang, One-step assembly of a biomimetic biopolymer coating for particle surface engineering, Adv. Mater. 30 (2018) 1802851.
[64] M.M. Rodrigues, C.P. Fontoura, A.E.D. Maddalozzo, L.M. Leidens, H.G. Quevedo, K. dos Santos Souza, J. da Silva Crespo, A.F. Michels, C.A. Figueroa, C. Aguzzoli, Ti, Zr and Ta coated UHMWPE aiming surface improvement for biomedical purposes, Compos. B. Eng., 189 (2020) 107909.
[65] H. Dong, T. Bell, C. Blawert, B. Mordike, Plasma immersion ion implantation of UHMWPE, J. Mater. Sci. Lett. 19 (2000) 1147–1149.
[66] G. Kaklamani, N. Mehrban, J. Chen, J. Bowen, H. Dong, L. Grover, A. Stamboulis, Effect of plasma surface modification on the biocompatibility of UHMWPE, Biomed. Mater. 5 (2010), 054102.
[67] M. Zaka-ul-Islam, M. Naeem, M. Shafiq, A.J. Al-Rajab, M. Zakaullah, Active screen cage pulsed dc discharge for implanting copper in polytetrafluoroethylene (PTFE), Mater. Res. Express 4 (2017), 075304.
[68] X. Fu, R.L. Sammons, I. Bertóti, M.J. Jenkins, H. Dong, Active screen plasma surface modification of polycaprolactone to improve cell attachment, J. Biomed. Mater. Res. 100 (2012) 314–320.
[69] X. Fu, M.J. Jenkins, G. Sun, I. Bertoti, H. Dong, Characterization of active screen plasma modified polyurethane surfaces, Surf. Coat. Technol. 206 (2012) 4799–4807.
[70] G. Kaklamani, J. Bowen, N. Mehrban, H. Dong, L.M. Grover, A. Stamboulis, Active screen plasma nitriding enhances cell attachment to polymer surfaces, Appl. Surf. Sci. 273 (2013) 787–798.
[71] G. Kaklamani, N. Mehrban, J. Bowen, H. Dong, L. Grover, A. Stamboulis, Nitrogen plasma surface modification enhances cellular compatibility of aluminosilicate glass, Mater. Lett. 111 (2013) 225–229.
[72] N. Mehrban, D. Cardinale, S.C. Gallo, D.D. Lee, D.A. Scott, H. Dong, J. Bowen, D. N. Woolfson, M.A. Birchall, C. O'Callaghan, α-Helical peptides on plasma-treated polymers promote ciliation of airway epithelial cells, Mater. Sci. Eng. C 122 (2021), 111935.
[73] S. Corujeira Gallo, H. Dong, New insights into the mechanism of low-temperature active-screen plasma nitriding of austenitic stainless steel, Scr. Mater. 67 (2012) 89–91.
[74] A. Saeed, A. Khan, F. Jan, M. Abrar, M. Khalid, M. Zakaullah, Validity of "sputtering and re-condensation" model in active screen cage plasma nitriding process, Appl. Surf. Sci. 273 (2013) 173–178.
[75] P.K. Chu, J. Chen, L. Wang, N. Huang, Plasma-surface modification of biomaterials, Mater. Sci. Eng. R. Rep. 36 (2002) 143–206.
[76] S.S. Silva, S.M. Luna, M.E. Gomes, J. Benesch, I. Pashkuleva, J.F. Mano, R.L. Reis, Plasma surface modification of chitosan membranes: characterization and preliminary cell response studies, Macromol. Biosci. 8 (2008) 568–576.
[77] N. Hattori, S. Yamada, K. Torii, S. Takeda, K. Nakamura, H. Tanaka, H. Kajiyama, M. Kanda, T. Fujii, G. Nakayama, Effectiveness of plasma treatment on pancreatic cancer cells, Int. J. Oncol. 47 (2015) 1655–1662.
[78] A. Lin, B. Truong, A. Pappas, L. Kirifides, A. Oubarri, S. Chen, S. Lin, D. Dobrynin, G. Fridman, A. Fridman, Uniform nanosecond pulsed dielectric barrier discharge plasma enhances anti-tumor effects by induction of immunogenic cell death in tumors and stimulation of macrophages, Plasma Process. Polym. 12 (2015) 1392–1399.
[79] R. Verloy, A. Privat-Maldonado, E. Smits, A. Bogaerts, Cold atmospheric plasma treatment for pancreatic cancer–the importance of pancreatic stellate cells, Cancers 12 (2020) 2782.
[80] S. Bekeschus, G. Liebelt, J. Menz, J. Berner, S.K. Sagwal, K. Wende, K.-D. Weltmann, L. Boeckmann, T. von Woedtke, H.-R. Metelmann, Tumor cell metabolism correlates with resistance to gas plasma treatment: the evaluation of three dogmas, Free Radic. Biol. Med. 167 (2021) 12–28.

[81] A.V. Nastuta, I. Topala, C. Grigoras, V. Pohoata, G. Popa, Stimulation of wound healing by helium atmospheric pressure plasma treatment, J. Phys. D. Appl. Phys. 44 (2011), 105204.

[82] R.S. Tipa, G.M. Kroesen, Plasma-stimulated wound healing, IEEE Trans. Plasma Sci. 39 (2011) 2978–2979.

[83] A. Schmidt, K. Wende, S. Bekeschus, L. Bundscherer, A. Barton, K. Ottmüller, K.-D. Weltmann, K. Masur, Non-thermal plasma treatment is associated with changes in transcriptome of human epithelial skin cells, Free Radic. Res. 47 (2013) 577–592.

[84] J.M. Jung, H.K. Yoon, C.J. Jung, S.Y. Jo, S.G. Hwang, H.J. Lee, W.J. Lee, S.E. Chang, C.H. Won, Cold plasma treatment promotes full-thickness healing of skin wounds in murine models, Int J Low Extrem Wounds, (2021) 15347346211002144.

[85] A. Schmidt, G. Liebelt, F. Nießner, T. von Woedtke, S. Bekeschus, Gas plasma-spurred wound healing is accompanied by regulation of focal adhesion, matrix remodeling, and tissue oxygenation, Redox Biol. 38 (2021), 101809.

[86] V. Cech, R. Prikryl, R. Balkova, A. Grycova, J. Vanek, Plasma surface treatment and modification of glass fibers, Compos. - A: Appl. Sci. Manuf. 33 (2002) 1367–1372.

[87] C. Cheng, Z. Liye, R.-J. Zhan, Surface modification of polymer fibre by the new atmospheric pressure cold plasma jet, Surf. Coat. Technol. 200 (2006) 6659–6665.

[88] B.-G. Cho, S.-H. Hwang, M. Park, J.K. Park, Y.-B. Park, H.G. Chae, The effects of plasma surface treatment on the mechanical properties of polycarbonate/carbon nanotube/carbon fiber composites, Compos. B. Eng. 160 (2019) 436–445.

[89] Y. Liang, X. Li, D. Semitekolos, C.A. Charitidis, H. Dong, Enhanced properties of PAN-derived carbon fibres and resulting composites by active screen plasma surface functionalisation, Plasma Process. Polym. 17 (2020) 1900252.

[90] R. Foerch, D. Hunter, Remote nitrogen plasma treatment of polymers: polyethylene, nylon 6, 6, poly (ethylene vinyl alcohol), and poly (ethylene terephthalate), J. Polym. Sci. A Polym. Chem. 30 (1992) 279–286.

[91] Z. Khosravi, S. Kotula, A. Lippitz, W.E. Unger, C.P. Klages, IR-and NEXAFS-spectroscopic characterization of plasma-nitrogenated polyolefin surfaces, Plasma Process. Polym. 15 (2018) 1700066.

[92] C. Rulison, So you want to measure surface energy, Kruss (1999) 1–16.

[93] R.N. Wenzel, Resistance of solid surfaces to wetting by water, Ind. Eng. Chem. Res. 28 (1936) 988–994.

[94] J.-M. Romano, J. Fantova Sarasa, C. Concheso, M. Gulcur, B. Dashtbozorg, A. Garcia-Giron, P. Penchev, H. Dong, B.R. Whiteside, S. Dimov, Effects of mould wear on hydrophobic polymer surfaces replicated using plasma-treated and laser-textured stainless steel inserts, Tribol. - Mater. Surf. Interfaces 14 (2020) 240–252.

[95] A. Cassie, S. Baxter, Wettability of porous surfaces, Trans. Faraday Soc. 40 (1944) 546–551.

[96] F.M. Etzler, Determination of the surface free energy of solids, Rev. Adhes. Adhes. 1 (2013) 3–45.

[97] T. Murakami, S.-i. Kuroda, Z. Osawa, Dynamics of polymeric solid surfaces treated with oxygen plasma: effect of aging media after plasma treatment, J. Colloid Interface Sci., 202 (1998) 37–44.

[98] S. Zanini, R. Barni, R. Della Pergola, C. Riccardi, Modification of the PTFE wettability by oxygen plasma treatments: influence of the operating parameters and investigation of the ageing behaviour, J. Phys. D. Appl. Phys. 47 (2014), 325202.

[99] J. Nakamatsu, L.F. Delgado-Aparicio, R. Da Silva, F. Soberon, Ageing of plasma-treated poly (tetrafluoroethylene) surfaces, J. Adhes. Sci. Technol. 13 (1999) 753–761.

[100] E. Liston, L. Martinu, M. Wertheimer, Plasma surface modification of polymers for improved adhesion: a critical review, J. Adhes. Sci. Technol. 7 (1993) 1091–1127.

[101] R. Morent, N. De Geyter, C. Leys, L. Gengembre, E. Payen, Study of the ageing behaviour of polymer films treated with a dielectric barrier discharge in air, helium and argon at medium pressure, Surf. Coat. Technol. 201 (2007) 7847–7854.

[102] A. Vesel, M. Mozetic, New developments in surface functionalization of polymers using controlled plasma treatments, J. Phys. D. Appl. Phys. 50 (2017), 293001.

[103] L. Ghasemi-Mobarakeh, D. Kolahreez, S. Ramakrishna, D. Williams, Key terminology in biomaterials and biocompatibility, Curr. Opin. Biomed. Eng. 10 (2019) 45–50.

[104] G. Altankov, T. Groth, Reorganization of substratum-bound fibronectin on hydrophilic and hydrophobic materials is related to biocompatibility, J. Mater. Sci. Mater. Med. 5 (1994) 732–737.

[105] Y.-X. Wang, J.L. Robertson, W.B. Spillman, R.O. Claus, Effects of the chemical structure and the surface properties of polymeric biomaterials on their biocompatibility, Pharm. Res. 21 (2004) 1362–1373.

[106] K.L. Menzies, L. Jones, The impact of contact angle on the biocompatibility of biomaterials, Optom. Vis. Sci. 87 (2010) 387–399.

[107] H.J. Griesser, R.C. Chatelier, T.R. Gengenbach, G. Johnson, J.G. Steele, Growth of human cells on plasma polymers: putative role of amine and amide groups, J. Biomater. Sci. Polym. Ed. 5 (1994) 531–554.

[108] J.G. Steele, G. Johnson, C. McFarland, B. Dalton, T. Gengenbach, R. Chatelier, P. A. Underwood, H. Griesser, Roles of serum vitronectin and fibronectin in initial attachment of human vein endothelial cells and dermal fibroblasts on oxygen-and nitrogen-containing surfaces made by radiofrequency plasmas, J. Biomater. Sci. Polym. Ed. 6 (1995) 511–532.

[109] H.P. Felgueiras, M.D. Evans, V. Migonney, Contribution of fibronectin and vitronectin to the adhesion and morphology of MC3T3-E1 osteoblastic cells to poly (NaSS) grafted Ti6Al4V, Acta Biomater. 28 (2015) 225–233.

[110] P. Mallick, Fiber-Reinforced Composites: Materials, Manufacturing, And Design, 2007.

[111] A.S. Aricò, P. Bruce, B. Scrosati, J.-M. Tarascon, W. van Schalkwijk, Nanostructured materials for advanced energy conversion and storage devices, Nat. Mater. 4 (2005) 366–377.

[112] A.G. Pandolfo, A.F. Hollenkamp, Carbon properties and their role in supercapacitors, J. Power Sources 157 (2006) 11–27.

[113] D. Chen, H. Feng, J. Li, Graphene oxide: preparation, functionalization, and electrochemical applications, Chem. Rev. 112 (2012) 6027–6053.

[114] M. Sharma, S. Gao, E. Mäder, H. Sharma, L.Y. Wei, J. Bijwe, Carbon fiber surfaces and composite interphases, Compos. Sci. Technol. 102 (2014) 35–50.

[115] D. Qu, Studies of the activated carbons used in double-layer supercapacitors, J. Power Sources 109 (2002) 403–411.

[116] K.L. Klein, A.V. Melechko, T.E. McKnight, S.T. Retterer, P.D. Rack, J.D. Fowlkes, D.C. Joy, M.L. Simpson, Surface characterization and functionalization of carbon nanofibers, Int. J. Appl. Phys. 103 (2008), 061301.

[117] Y. Shao, J. Wang, M. Engelhard, C. Wang, Y. Lin, Facile and controllable electrochemical reduction of graphene oxide and its applications, J. Mater. Chem. 20 (2010) 743–748.

[118] S. Corujeira Gallo, C. Charitidis, H. Dong, Surface functionalization of carbon fibers with active screen plasma, J. Vac. Sci. Technol. 35 (2017), 021404.

[119] D. Semitekolos, A.-F. Trompeta, I. Husarova, T. Man'ko, A. Potapov, O. Romenskaya, Y. Liang, X. Li, M. Giorcelli, H. Dong, A. Tagliaferro, C.A. Charitidis, Comparative physical–mechanical properties assessment of tailored surface-treated carbon fibres, Materials, 13 (2020).

[120] S. Du, K. Lin, S.K. Malladi, Y. Lu, S. Sun, Q. Xu, R. Steinberger-Wilckens, H. Dong, Plasma nitriding induced growth of Pt-nanowire arrays as high performance electrocatalysts for fuel cells, Sci. Rep. 4 (2014) 6439.

[121] K. Lin, Y. Lu, S. Du, X. Li, H. Dong, The effect of active screen plasma treatment conditions on the growth and performance of Pt nanowire catalyst layer in DMFCs, Int. J. Hydrog. Energy 41 (2016) 7622–7630.

[122] S. Corujeira Gallo, X. Li, K. Fütterer, C.A. Charitidis, H. Dong, Carbon nanofibers functionalized with active screen plasma-deposited metal nanoparticles for electrical energy storage devices, ACS Appl, Mater. Interfaces 9 (2017) 23195–23201.

[123] J. Chen, X. Shi, S. Qi, M. Mohai, I. Bertóti, Y. Gao, H. Dong, Reducing and multiple-element doping of graphene oxide using active screen plasma treatments, Carbon 95 (2015) 338–346.

[124] Z. Jing, S. Qi, X. Tao, H. Yu, W. Zhang, Y. Qiao, X. Li, H. Dong, Active-screen plasma multi-functionalization of graphene oxide for supercapacitor application, J. Mater. Sci. 56 (2021) 3296–3311.

[125] D.B. Schuepfer, F. Badaczewski, J.M. Guerra-Castro, D.M. Hofmann, C. Heiliger, B. Smarsly, P.J. Klar, Assessing the structural properties of graphitic and non-graphitic carbons by Raman spectroscopy, Carbon 161 (2020) 359–372.

[126] S. Mujin, H. Baorong, W. Yisheng, T. Ying, H. Weiqiu, D. Youxian, The surface of carbon fibres continuously treated by cold plasma, Compos. Sci. Technol. 34 (1989) 353–364.

[127] B.Z. Jang, Control of interfacial adhesion in continuous carbon and kevlar fiber reinforced polymer composites, Compos. Sci. Technol. 44 (1992) 333–349.

[128] Y. Liang, Enhancement and Evaluation of PAN-derived Carbon Fibres and Resulting Composites by Active Screen Plasma Surface Modification (PhD Thesis), University of Birmingham, Department of Metallurgy & Materials, 2021.

[129] M. Rybin, A. Pereyaslavtsev, T. Vasilieva, V. Myasnikov, I. Sokolov, A. Pavlova, E. Obraztsova, A. Khomich, V. Ralchenko, E. Obraztsova, Efficient nitrogen doping of graphene by plasma treatment, Carbon 96 (2016) 196–202.

[130] A.S. Biró, Active Screen Plasma Nitriding State of the Art, Production Processes and Systems, 7(1) 103–114.

[131] H. Dong, X. Li, Y. Dong, L. Tian, Method for Producing Long-Lasting Antibacterial Metallic Surfaces, European Patent: EP2870269, WO 2014/006390, 2020.